

Hypergeometric Systems in two Variables, Quivers, Dimers and Dessins d'Enfants.

Jan Stienstra

Mathematisch Instituut, Universiteit Utrecht, the Netherlands

e-mail: stien@math.uu.nl

Abstract

This paper presents some parallel developments in Quiver/Dimer Models, Hypergeometric Systems and Dessins d'Enfants. It demonstrates that the setting in which Gelfand, Kapranov and Zelevinsky have formulated the theory of hypergeometric systems, provides also a natural setting for dimer models. The Fast Inverse Algorithm of [14] and the untwisting procedure of [4] are recasted in this more natural setting and then immediately produce from the quiver data the Kasteleyn matrix for dimer models, which is best viewed as the bi-adjacency matrix for the untwisted model. Some perfect matchings in the dimer models are direct reformulations of the triangulations in GKZ theory and the rule which maps triangulations to the vertices of the secondary polygon extends to a rule for mapping perfect matchings to lattice points in the secondary polygon. Finally it is observed in many examples and then conjectured to hold in general, that the determinant of the Kasteleyn matrix with suitable weights becomes after a simple transformation equal to the principal \mathcal{A} -determinant in GKZ theory. Illustrative examples are distributed throughout the text.

1 Introduction

In the last decade interesting correspondences were discovered relating Quiver Gauge Theories, lattice polygons and Calabi-Yau singularities. The motivation and evolution of these ideas in physics are well-documented in many articles; e.g. [1, 3, 4, 5, 6, 12, 13, 14, 15, 16, 17, 19, 20]. In the present paper we want to put some aspects of these correspondences from physics alongside the hypergeometric systems in two variables of Gelfand, Kapranov, Zelevinsky [8, 9, 10] and the dessins d'enfants of Grothendieck et al. [18, 22, 24]. This reveals intriguing connections between these fields.

The beautiful insight of Gelfand, Kapranov and Zelevinsky was that hypergeometric structures greatly simplify if one introduces extra variables and balances this with an appropriate torus action [8, 9, 10, 11, 25]. In order to profit from the simplification they developed tools like the *secondary fan*, *secondary polytope* and *principal \mathcal{A} -determinant*. This paper demonstrates that these are also very practical tools for studying quivers and dimer models.

A similar beautiful insight of simplification by going to higher dimensions appeared in De Bruijn's construction [2] of Penrose tilings and developed into the well-known projection method in the theory of quasi-crystals; e.g. [23]. We apply the same method to construct periodic rhombus tilings of the plane, which the physicists call *brane tilings* and *dimer models*.

From a geometric perspective this paper deals with embeddings of quivers into compact oriented surfaces without boundary. More specifically, the initial combinatorial data for a quiver \mathbf{Q} are two finite sets E (arrows) and V (nodes) and two maps $s, t : E \rightarrow V$ (source and target). Embedding \mathbf{Q} into a compact oriented surface without boundary \mathcal{M} means that V becomes a subset of \mathcal{M} and an arrow $e \in E$ becomes a path p_e in \mathcal{M} from the point $s(e)$ to the point $t(e)$. It is required that the boundary of every *face of* $(\mathcal{M}, \mathbf{Q})$ – i.e. connected component of $\mathcal{M} \setminus \bigcup_{e \in E} p_e$ – is formed by a sequence of paths $(p_{e_1}, \dots, p_{e_n})$ with $p_{e_i} \cap p_{e_{i+1}} = t(e_i) = s(e_{i+1})$ for $1 \leq i \leq n$; $e_{n+1} = e_1$. It is evident from this requirement that the face boundaries receive an orientation from \mathbf{Q} . When this is combined with the orientation on \mathcal{M} faces lie either on the positive or on the negative side of their boundary. In pictures we mark faces which lie on the positive (respectively negative) side of their boundary with \bullet (resp. \circ). It is obvious that adjacent faces get different colors. The dual graph of \mathbf{Q} w.r.t. \mathcal{M} is thus a bi-partite graph $\Gamma^{\bullet\circ}$, embedded in \mathcal{M} : the nodes of $\Gamma^{\bullet\circ}$ correspond with the faces of $(\mathcal{M}, \mathbf{Q})$; the edges of $\Gamma^{\bullet\circ}$ connect nodes coming from adjacent faces and correspond bijectively with the edges of \mathbf{Q} . A pair $(\mathcal{M}, \mathbf{Q})$ consisting of a compact oriented surface without boundary and an oriented graph embedded in it is called a *dessin d'enfants* or just *dessin*, in one of the various equivalent definitions of “dessin (d'enfants)”; see [22, 18, 24]. Other definitions refer to $(\mathcal{M}, \Gamma^{\bullet\circ})$ as dessin d'enfants. In case \mathcal{M} has genus 1 one often calls $\Gamma^{\bullet\circ}$ and its lifting to the plane (i.e. the universal covering of the torus \mathcal{M}) a *dimer model* or *brane tiling*; see for instance [4, 5, 12, 13, 14, 15]. Yet another presentation of the same structure gives the dessin as the triangulation of \mathcal{M} with vertex set the union of the nodes of \mathbf{Q} and $\Gamma^{\bullet\circ}$; the triangles are given by the triplets of vertices consisting of two nodes of $\Gamma^{\bullet\circ}$ connected by an edge e^* of $\Gamma^{\bullet\circ}$ and one node v of \mathbf{Q} incident to the edge e of \mathbf{Q} which is dual to e^* . Figure 1 shows these three get-ups of the dessin d'enfants of the \mathbb{P}^2 -quiver (case B_1 in Figure 3)

From an algebraic perspective this paper deals with *superpotentials for quivers*. There is a simple equivalence between the geometric and algebraic

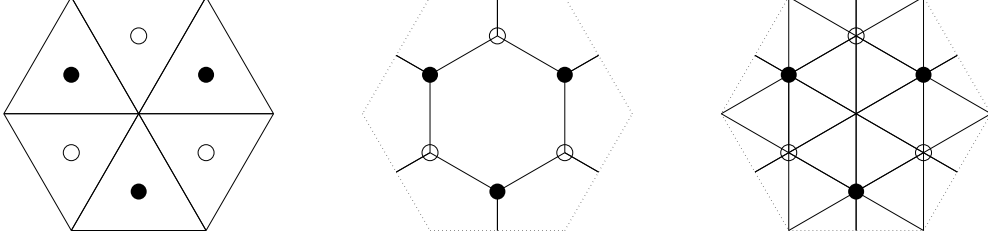


Figure 1: *Three versions of the dessin d'enfants for \mathbb{P}^2 (= case B_1 in Fig. 3). The surface is obtained by identifying opposite sides of the hexagon.*

perspectives: the superpotential is a convenient way of writing the list of oriented boundaries $(p_{e_1}, \dots, p_{e_n})$ of the faces of $(\mathcal{M}, \mathcal{Q})$ with \pm -signs indicating how the orientation matches with that of \mathcal{M} . It can also be read as the instruction for building \mathcal{M} by glueing polygons. For the dessin d'enfants in Figure 1 the superpotential (for some numbering of the arrows of \mathcal{Q}) is

$$X_1 X_2 X_3 + X_4 X_5 X_6 + X_7 X_8 X_9 - X_2 X_8 X_5 - X_3 X_9 X_6 - X_4 X_1 X_7.$$

Another algebraic perspective, equivalent to the previous one, is given by what we want to call *the bi-adjacency matrix of the dessin d'enfants $(\mathcal{M}, \mathcal{Q})$ with weight ϖ* . It is defined as follows. The *weight* is a function $\varpi : E \rightarrow \mathbb{C}$. The dessins in the present paper have as many black faces as white faces and every edge $e \in E$ lies in the boundary of a unique black face, denoted $\mathbf{b}(e)$, and a unique white face, denoted $\mathbf{w}(e)$. The bi-adjacency matrix of $(\mathcal{M}, \mathcal{Q})$ with weight ϖ is a square matrix \mathbb{K}^ϖ with rows corresponding with the black faces, columns corresponding with the white faces and entries in the polynomial ring $\mathbb{C}[u_v \mid v \in V]$ which has one variable for every node v of the quiver \mathcal{Q} : *the (\mathbf{b}, \mathbf{w}) -entry of \mathbb{K}^ϖ is*

$$\mathbb{K}_{\mathbf{b}, \mathbf{w}}^\varpi = \sum_{e \in E: \mathbf{b}(e)=\mathbf{b}, \mathbf{w}(e)=\mathbf{w}} \varpi(e) u_{s(e)} u_{t(e)}. \quad (1)$$

The bi-adjacency matrix is in fact the *Kasteleyn matrix* of a twist of the dimer model $(\mathcal{M}, \Gamma^{\bullet\circ})$; see Section 8. For the dessin in Figure 1 the bi-adjacency matrix (for some numbering of the nodes, edges and faces) is

$$\begin{bmatrix} \varpi_1 u_1 u_3 & \varpi_2 u_1 u_2 & \varpi_3 u_2 u_3 \\ \varpi_4 u_2 u_3 & \varpi_5 u_1 u_3 & \varpi_6 u_1 u_2 \\ \varpi_7 u_1 u_2 & \varpi_8 u_2 u_3 & \varpi_9 u_1 u_3 \end{bmatrix}.$$

In Section 2 we describe how the quivers for which we can solve the embedding problem, are associated with certain rank 2 subgroups \mathbb{L} of \mathbb{Z}^N ; here N is the number of nodes of the quiver. Such subgroups $\mathbb{L} \subset \mathbb{Z}^N$ are the

foundations for the theory of Gelfand, Kapranov and Zelevinsky. In Section 3 we describe the *secondary fan* and the *secondary polygon* associated with $\mathbb{L} \subset \mathbb{Z}^N$. These important structures in GKZ-theory surprisingly turn out to be also quite relevant for the dimer models. We show for instance in Theorem 9.3 that the secondary polygon is the *Newton polygon* of the determinant of the bi-adjacency matrix with non-zero weights. In Section 10 we report the observation, based on examples, that for the *critical weight*

$$\text{crit} : E \rightarrow \mathbb{Z}_{>0}, \quad \text{crit}(e) = \#\{e' \in E \mid s(e') = s(e), t(e') = t(e)\} \quad (2)$$

the determinant of the bi-adjacency matrix \mathbb{K}^{crit} , after a simple transformation, becomes equal to the *principal \mathcal{A} -determinant* of Gelfand, Kapranov, Zelevinsky [11]. In Sections 4 and 5 we recall some topics in the theory of GKZ-hypergeometric systems of differential equations.

Section 6 presents the algorithm to solve the quiver embedding problem. It is a combination of the *Fast Inverse Algorithm* of [14] and the *untwisting procedure* of [4]. In the cited papers, however, methods are mainly presented via visual inspection of pictures in some concrete examples. So an extrapolation to general situations was needed. The first impression that the Fast Inverse Algorithm of [14] is more or less De Bruijn's construction [2] of Penrose tilings did not quite yield the sought after embedding of the quiver; the untwisting procedure of [4] is also needed. The algorithm became a smoothly operating algebraic-combinatorial tool by consistently working from the philosophy that things look simpler from a higher dimensional viewpoint (with group action). For doing the computer experiments behind this paper I implemented the algorithm in MATLAB. The reader can find in Section 6 sufficient details for making a computer version of the algorithm.

Sections 7–10 demonstrate that consistently working from the higher dimensional viewpoint leads to new insights in the dimer technology tools *perfect matchings*, *Kasteleyn matrix and its determinant* and shows their close relation with the GKZ tools *secondary polytope* and *principal \mathcal{A} -determinant*.

Besides problems such as proving that the algorithm of Section 6 yields at least one superpotential for every quiver which satisfies the conditions in Theorem 2.10, or proving Conjecture 10.5 our work raises some interesting questions like:

Q1. The Calabi-Yau singularities in the background of this work are constructed from toric diagrams, which here are interpreted as secondary polygons. In [19] §6 the singularity is obtained from the toric diagram by a symplectic quotient construction. In [12] §2 the singularity is given as a toric variety constructed from a fan with one maximal cone, namely the cone over the toric diagram (polygon). For this the polygon is put into the plane of points with first coordinate 1 in \mathbb{R}^3 . In the work of Gelfand, Kapranov and Zelevinsky the secondary polygon is put into a 2-dimensional plane in

\mathbb{R}^N , which does not pass through $\mathbf{0}$; here N is the number of nodes of the quiver. One can perform the standard toric variety construction with the 3-dimensional cone over the secondary polygon in \mathbb{R}^N . *Does this toric variety give the appropriate view in the GKZ philosophy (higher dimension compensated by group action) on the singular Calabi-Yau 3-space?* Since this toric variety is a natural domain for GKZ hypergeometric functions (see 5.2) one may wonder: *Do hypergeometric functions provide new useful tools for investigating the geometry of 3-dimensional Calabi-Yau singularities?* Possibly positive indications are the fact that the dimension of the solution space of the GKZ system of hypergeometric differential equations equals the size of the bi-adjacency matrix \mathbb{K}^{crit} (see Theorem 5.3 and Corollary 7.3) and the observation (Conjecture 10.5) that the determinant of \mathbb{K}^{crit} equals, up to a simple transformation, the principal \mathcal{A} -determinant, which describes the singularities of the GKZ system.

Q2. The surface \mathcal{M} with embedded in it the pair of dual graphs \mathbf{Q} and $\Gamma^{\bullet\circ}$ has been constructed in a purely combinatorial topological way from the superpotential. It is a general fact (see [18] §1.2) that there is then a continuous map f from \mathcal{M} to the 2-sphere S^2 which is a ramified covering with exactly three ramification points such that the set of vertices of \mathbf{Q} , the set of black vertices of $\Gamma^{\bullet\circ}$ and the set of white vertices of $\Gamma^{\bullet\circ}$ are the fibers over the three ramification points. A highlight in the theory of dessins d'enfants is *Belyi's Theorem* (see [18] Theorem 2.1.1). It states that in the above situation the surface \mathcal{M} admits a model \mathcal{M}_K over a number field K such that f becomes a morphism $\mathcal{M}_K \rightarrow \mathbb{P}_K^1$ of algebraic curves over K which is unramified outside $\{0, 1, \infty\}$. The labeling of the ramification points can be taken such that $f^{-1}(\infty)$, $f^{-1}(0)$ and $f^{-1}(1)$ are the sets of white and black vertices of $\Gamma^{\bullet\circ}$ and the vertices of \mathbf{Q} , respectively. The bipartite graph $\Gamma^{\bullet\circ}$ in \mathcal{M} is then the inverse image of the negative real axis $[-\infty, 0]$ in the Riemann sphere $\mathbb{P}_{\mathbb{C}}^1 = S^2$ and the quiver \mathbf{Q} is the inverse image of the positively oriented unit circle $\{z \in \mathbb{C} \mid |z| = 1\}$. It is usually difficult to find explicit algebraic equations for \mathcal{M}_K and the *Belyi function* f .

On the other hand, the authors of [4] write in footnote ⁶: *we have produced a dimer model that is defined on its own spectral curve $\det \mathbb{K}^{\varpi} = 0$.* Unfortunately their arguments are not (yet) sufficiently refined to yield the weight ϖ that is to be used in this equation.

It seems an interesting challenge to tackle the two problems simultaneously and look for a weight ϖ and a Belyi function f on the algebraic curve with equation $\det \mathbb{K}^{\varpi} = 0$ that realize $(\mathcal{M}, \mathbf{Q}, \Gamma^{\bullet\circ})$ as described above.

2 Rank 2 subgroups of \mathbb{Z}^N and Quivers.

2.1. The most basic object in this paper is a rank 2 subgroup $\mathbb{L} \subset \mathbb{Z}^N$ which is not contained in any of the standard coordinate hyperplanes of \mathbb{Z}^N and is perpendicular to the vector $(1, \dots, 1)$, with all coordinates 1. So, the elements of \mathbb{L} are vectors $(\ell_1, \dots, \ell_N) \in \mathbb{Z}^N$ with $\ell_1 + \dots + \ell_N = 0$ and for every $i \in \{1, \dots, N\}$ there is an $(\ell_1, \dots, \ell_N) \in \mathbb{L}$ such that $\ell_i \neq 0$.

2.2. Notation. Throughout this paper $\mathbf{e}_1, \dots, \mathbf{e}_N$ is the standard basis of \mathbb{Z}^N and J denotes the matrix $\begin{pmatrix} 0 & 1 \\ -1 & 0 \end{pmatrix}$.

2.3. Definition/construction. Taking the second exterior powers one finds an inclusion $\bigwedge^2 \mathbb{L} \hookrightarrow \bigwedge^2 \mathbb{Z}^N$. The group $\bigwedge^2 \mathbb{L}$ is a free \mathbb{Z} -module of rank 1. After fixing the orientation on \mathbb{L} , i.e. choosing one of the two possible isomorphisms $\bigwedge^2 \mathbb{L} \simeq \mathbb{Z}$, one gets an inclusion $\mathbb{Z} \hookrightarrow \bigwedge^2 \mathbb{Z}^N$. The coordinates of $1 \in \mathbb{Z}$ with respect to the standard basis $\{\mathbf{e}_i \wedge \mathbf{e}_j\}_{1 \leq i < j \leq N}$ of $\bigwedge^2 \mathbb{Z}^N$ are called the *Plücker coordinates* of $\mathbb{L} \subset \mathbb{Z}^N$.

Dual to the above inclusion one finds the map $\bigwedge^2 \mathbb{Z}^N \rightarrow \mathbb{Z}$, i.e. an anti-symmetric bilinear form on \mathbb{Z}^N . In view of its relation with the Plücker coordinates we call this the *Plücker form* of \mathbb{L} .

To make this look more explicit we take a basis for \mathbb{L} compatible with the chosen orientation. One can represent the two basis vectors as the rows of a $2 \times N$ -matrix B . Let $\mathbf{b}_1, \dots, \mathbf{b}_N$ be the columns of this matrix. Then the Plücker coordinates are $(\det(\mathbf{b}_i, \mathbf{b}_j))_{1 \leq i < j \leq N}$ and the (anti-symmetric) matrix for the Plücker form is $(\det(\mathbf{b}_i, \mathbf{b}_j))_{1 \leq i, j \leq N}$. The Plücker coordinates and the Plücker form do, of course, not change if one takes another basis for \mathbb{L} with the same orientation. Note that the matrix for the Plücker form has rank 2:

$$\text{rank} ((\det(\mathbf{b}_i, \mathbf{b}_j))_{1 \leq i, j \leq N}) = 2. \quad (3)$$

2.4. Definition. A *quiver* Q is a finite directed graph. It can be given combinatorially by two finite sets E and V and two maps $s, t : E \rightarrow V$; in short hand notation $Q = (E, V, s, t)$. Each element of V is a node of the graph and an element $e \in E$ is an arrow from node $s(e)$ to node $t(e)$. The *adjacency matrix* of the quiver is the matrix $(q_{ij})_{i, j \in V}$ with entry q_{ij} equal to the number of arrows from node i to node j . If the quiver has no directed loops of length ≤ 2 (i.e. $q_{ij}q_{ji} = 0$ for all $i, j \in V$), it is faithfully described by the *anti-symmetrized adjacency matrix* $Q = (q_{ij} - q_{ji})_{i, j \in V}$. If the (i, j) -entry of Q is positive it equals the number of arrows from node i to node j . If it is negative it is the number of arrows from j to i .

2.5. Definition. We call the quiver without directed loops of length ≤ 2 with anti-symmetrized adjacency matrix equal to the matrix of the Plücker form of \mathbb{L} the *Plücker quiver of \mathbb{L}* .

2.6. Examples of groups $\mathbb{L} \subset \mathbb{Z}^N$ and their Plücker quivers are shown in Figures 3 and 4.

2.7. Some easily visible geometric properties of a quiver without directed loops of length ≤ 2 are equivalent to easily seen algebraic properties of its anti-symmetrized adjacency matrix Q . For instance, the graph has no isolated nodes if and only if no column of Q is zero. Also, in every node of the quiver the number of incoming arrows equals the number of outgoing arrows precisely if in each row of Q the sum of the entries is 0. For Plücker quivers these properties correspond to the conditions that \mathbb{L} is not contained in any of the standard coordinate hyperplanes of \mathbb{Z}^N and is perpendicular to the vector $(1, \dots, 1)$. One property of a Plücker quiver which one can not easily read off from the graph is $\text{rank } Q = 2$.

In the remainder of this section we show that these properties characterize Plücker quivers of rank 2 subgroups $\mathbb{L} \subset \mathbb{Z}^N$ as in 2.1.

2.8. Proposition. *An $N \times N$ -matrix C with entries in \mathbb{Z} is anti-symmetric and $\text{rank } C = 2$ if and only if there is a $2 \times N$ -matrix B with entries in \mathbb{Z} such that $\text{rank } B = 2$ and $C = B^t J B$.*

Proof. The “if”-statement is trivial. So let us consider the “only if” and assume that C is anti-symmetric and $\text{rank } C = 2$. Let d denote the greatest common divisor of the entries of C and $C' = \frac{1}{d}C$. Choose an $N \times 2$ -matrix D whose columns form a \mathbb{Z} -basis for the column space of C' . The equality of column spaces of C' and D means that there are an $N \times 2$ -matrix E and a $2 \times N$ -matrix F , both with entries in \mathbb{Z} and of rank 2, such that $D = C'E$ and $C' = DF$. Then $C' = DF = C'EF = -C'^t EF = -F^t D^t EF$. So $D^t E$ is an anti-symmetric 2×2 -matrix; say $D^t E = fJ$ with $f \in \mathbb{Z}$. In fact $f = \pm 1$ since it divides all entries of C' . If $f = 1$ we replace F by JF . We then always have $C' = F^t J F$. Let G be any 2×2 -matrix with entries in \mathbb{Z} and $\det G = d$. Let $B = GF$. Then $C = B^t J B$ as wanted. ■

2.9. Multiplying in Proposition 2.8 the matrix B from the left by a matrix from $SL_2(\mathbb{Z})$ does not change the matrix $B^t J B$. So it is more natural to interpret C as the matrix of the Plücker form of the \mathbb{Z} -row space of B . Note that it follows from the proof of Proposition 2.8 that this space is uniquely determined if the greatest common divisor of the entries of C is 1. If on the other hand the greatest common divisor of the entries of C is $d > 1$ this space depends on the additional choice of a 2×2 -matrix with entries in \mathbb{Z}

and determinant d .

Let us summarize the above discussion:

2.10. Theorem. *For every $\mathbb{L} \subset \mathbb{Z}^N$ as in 2.1 one has its Plücker quiver. This quiver has no isolated nodes or directed loops of length ≤ 2 and in every node the number of incoming arrows equals the number of outgoing arrows. Moreover the rank of its anti-symmetrized adjacency matrix is 2. Conversely, every quiver with these properties is the Plücker quiver of some $\mathbb{L} \subset \mathbb{Z}^N$ as in 2.1. The correspondence between such quivers and such $\mathbb{L} \subset \mathbb{Z}^N$ is one-to-one for those quivers for which the greatest common divisor of the entries of the anti-symmetrized adjacency matrix is 1 and those $\mathbb{L} \subset \mathbb{Z}^N$ for which \mathbb{Z}^N/\mathbb{L} has no torsion. ■*

3 The secondary fan and polygon of $\mathbb{L} \subset \mathbb{Z}^N$.

3.1. For $\mathbb{L} \subset \mathbb{Z}^N$ as in 2.1 we now define the *secondary fan* and the *secondary polytope*. In 4.12 we will compare this with the original definitions by Gelfand, Kapranov and Zelevinsky. The term “secondary” refers to the fact that in their theory of hypergeometric systems another polytope appears first, which is therefore called the *primary polytope*. Nonetheless both the secondary fan and the secondary polytope can most conveniently and directly be described using the lattice \mathbb{L} . In case the rank of \mathbb{L} is 2, the constructions become particularly simple.

3.2. Definition. Let $\mathbb{L} \subset \mathbb{Z}^N$ be as in 2.1. Let $\mathbb{L}_{\mathbb{R}}^{\vee} := \text{Hom}(\mathbb{L}, \mathbb{R})$ denote the real dual space of \mathbb{L} . Let $\mathbf{e}_1, \dots, \mathbf{e}_N$ be the standard basis of \mathbb{Z}^N . Let $\mathbf{b}_i \in \mathbb{L}_{\mathbb{R}}^{\vee}$ be the image of \mathbf{e}_i under the map $\mathbb{R}^N \rightarrow \mathbb{L}_{\mathbb{R}}^{\vee}$ dual to the inclusion $\mathbb{L} \hookrightarrow \mathbb{Z}^N$. Here and henceforth we identify \mathbb{R}^N with the real dual space of \mathbb{Z}^N by means of the standard dot product.

By definition, the *secondary fan of \mathbb{L}* is the following collection of cones in $\mathbb{L}_{\mathbb{R}}^{\vee}$: the 0-dimensional cone $\{\mathbf{0}\}$, the 1-dimensional cones $\mathbb{R}_{\geq 0}\mathbf{b}_i$ ($i = 1, \dots, N$) and the 2-dimensional cones which are the closures of the connected components of $\mathbb{L}_{\mathbb{R}}^{\vee} \setminus \bigcup_{i=1}^N \mathbb{R}_{\geq 0}\mathbf{b}_i$.

3.3. Definition. With a 2-dimensional cone C in the secondary fan one associates the set

$$L_C := \{ \{i, j\} \subset \{1, \dots, N\} \mid C \subset (\mathbb{R}_{\geq 0}\mathbf{b}_i + \mathbb{R}_{\geq 0}\mathbf{b}_j) \} \quad (4)$$

of 2-element subsets of $\{1, \dots, N\}$ and the vector

$$\psi_C := \sum_{\{i,j\} \in L_C} |\det(\mathbf{b}_i, \mathbf{b}_j)| (\mathbf{e}_i + \mathbf{e}_j). \quad (5)$$

The *secondary polytope* $\Sigma(\mathbb{L})$ of $\mathbb{L} \subset \mathbb{Z}^N$ is then defined as

$$\Sigma(\mathbb{L}) := \text{convex hull}(\{\psi_C \mid C \text{ 2-dim cone of secondary fan}\}).$$

3.4. Remark. In §4.12 we give an interpretation of the above L_C as a triangulation of the primary polytope. In Equation (27) we associate with L_C a perfect matching in a bipartite graph.

3.5. Example. Figure 2 shows the secondary fan with the lists L_C , the secondary polytope $\Sigma(\mathbb{L})$ with coordinates for the vertices and the primary polytope for $\mathbb{L} = \mathbb{Z}(0, 1, 1, -2) \oplus \mathbb{Z}(-1, 0, 2, -1) \subset \mathbb{Z}^4$. This is case B_2 of Figure 3; see also Example 4.6 and §4.12.

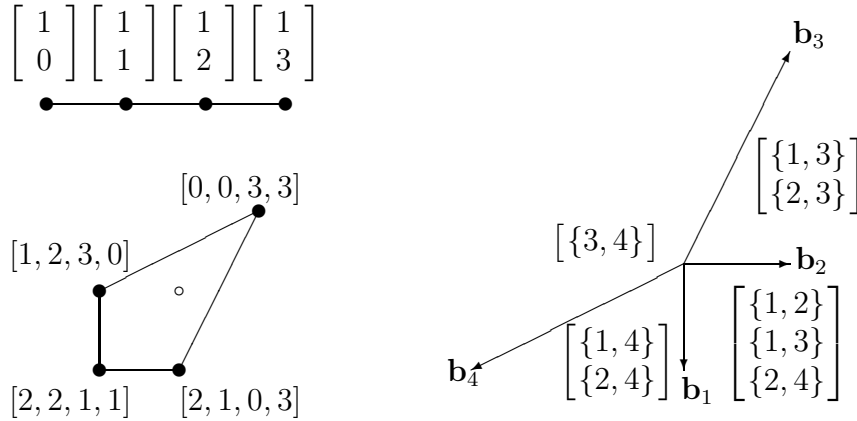


Figure 2: The secondary fan (right) and the primary polytope (top left) and the secondary polytope (bottom left) for $\mathbb{L} = \mathbb{Z}(0, 1, 1, -2) \oplus \mathbb{Z}(-1, 0, 2, -1) \subset \mathbb{Z}^4$.

3.6. The geometric formulation of the construction of the secondary fan and polytope is quite attractive. Nonetheless in practical algorithms everything can be most easily obtained from the matrix of the Plücker form of $\mathbb{L} \subset \mathbb{Z}^N$. Indeed, a 2-dimensional cone in the secondary fan is bounded by two half-lines $\mathbb{R}_{\geq 0}\mathbf{b}_i$ and $\mathbb{R}_{\geq 0}\mathbf{b}_j$ with the property that $\det(\mathbf{b}_i, \mathbf{b}_j) > 0$ and $\det(\mathbf{b}_i, \mathbf{b}_k) \det(\mathbf{b}_j, \mathbf{b}_k) \geq 0$ for $k = 1, \dots, N$. Thus to find the secondary fan one just needs to find all pairs $\mathbf{b}_i, \mathbf{b}_j$ with these properties.

For a cone C bounded by $\mathbb{R}_{\geq 0}\mathbf{b}_i$ and $\mathbb{R}_{\geq 0}\mathbf{b}_j$ the list L_C is then

$$L_C = \{ \{k, l\} \mid \det(\mathbf{b}_k, \mathbf{b}_i) \geq 0 \text{ and } \det(\mathbf{b}_j, \mathbf{b}_l) \geq 0 \}.$$

Now consider two adjacent 2-dimensional cones in the secondary fan, say C and C' . Let $\mathbf{b}_{i_1}, \dots, \mathbf{b}_{i_s}$ be those vectors from the set $\{\mathbf{b}_1, \dots, \mathbf{b}_N\}$ that lie on the half-line $C \cap C'$. Without loss of generality we may assume C lies to the right of \mathbf{b}_{i_1} and C' to the left. Then

$$\begin{aligned} L_C \setminus (L_C \cap L_{C'}) &= \{ \{k, l\} \mid l \in \{i_1, \dots, i_s\}, \det(\mathbf{b}_l, \mathbf{b}_k) < 0 \}, \\ L_{C'} \setminus (L_C \cap L_{C'}) &= \{ \{k, l\} \mid l \in \{i_1, \dots, i_s\}, \det(\mathbf{b}_l, \mathbf{b}_k) > 0 \}. \end{aligned}$$

From this we see, using $\sum_{k=1}^N \det(\mathbf{b}_i, \mathbf{b}_k) = 0$ for all i , that

$$\psi_{C'} - \psi_C = \sum_{r=1}^s \sum_{k=1}^N \det(\mathbf{b}_{i_r}, \mathbf{b}_k) \mathbf{e}_k. \quad (6)$$

In other words, $\psi_{C'} - \psi_C$ is the sum of rows i_1, \dots, i_s of the matrix of the Plücker form.

3.7. To make this even more explicit and simple looking we take a basis for \mathbb{L} compatible with the chosen orientation. One can represent the two basis vectors as the rows of a $2 \times N$ -matrix B . Let $\mathbf{b}_1, \dots, \mathbf{b}_N$ be the columns of this matrix. The elements of \mathbb{L} should now be written as row vectors with two components and the embedding $\mathbb{L} \hookrightarrow \mathbb{Z}^N$ is given by $\mathbf{v} \mapsto \sum_{k=1}^N (\mathbf{v} \cdot \mathbf{b}_k) \mathbf{e}_k$. Since $\det(\mathbf{b}_i, \mathbf{b}_k) = \mathbf{b}_i^t \mathbf{J} \mathbf{b}_k$, we can reformulate Equation (6) as

$$\psi_{C'} - \psi_C = \text{image of } \sum_{r=1}^s \mathbf{b}_{i_r}^t \mathbf{J} \text{ under the embedding } \mathbb{L} \hookrightarrow \mathbb{Z}^N. \quad (7)$$

In order to obtain the simplest formulation for the construction we order the vectors $\mathbf{b}_1, \dots, \mathbf{b}_N$ so that the points $\mathbf{p}_k = \sum_{i=1}^k \mathbf{b}_i^t$ for $k = 1, \dots, N$ lie ordered counterclockwise on the boundary of the polygon

$$\Delta = \text{convex hull}\{\mathbf{p}_1, \dots, \mathbf{p}_N\}. \quad (8)$$

Then the secondary polygon $\Sigma(\mathbb{L})$ is obtained by first rotating Δ clockwise over 90° , next embedding it along with \mathbb{L} into \mathbb{Z}^N and finally translating it over the vector ψ_C , where C is the cone in the secondary fan with left hand boundary $\mathbb{R}_{\geq 0}\mathbf{b}_1$.

Note that while the secondary polytope $\Sigma(\mathbb{L})$ depends only on the embedding $\mathbb{L} \hookrightarrow \mathbb{Z}^N$, the polygon Δ usually changes when one puts another vector \mathbf{b}_i in first position by a cyclic permutation or when one multiplies the vectors $\mathbf{b}_1, \dots, \mathbf{b}_N$ by a matrix from $Sl_2(\mathbb{Z})$.

3.8. For a converse to the above construction we start from a convex polygon Δ in \mathbb{R}^2 with vertices in \mathbb{Z}^2 and non-empty interior. Let $\partial\Delta$ denote its boundary. Next we choose a collection of points $\mathbf{p}_1, \dots, \mathbf{p}_N$ in $\partial\Delta \cap \mathbb{Z}^2$ which includes all vertices of Δ . We number these points so that \mathbf{p}_i and \mathbf{p}_{i+1} are consecutive points in the counter-clockwise orientation of $\partial\Delta$. Thinking of the elements of \mathbb{Z}^2 as row vectors we define column vectors $\mathbf{b}_1 = \mathbf{p}_1^t$ and $\mathbf{b}_i = \mathbf{p}_i^t - \mathbf{p}_{i-1}^t$ for $i = 2, \dots, N$. Finally we define \mathbb{L} to be the \mathbb{Z} -row space of the $2 \times N$ -matrix B with columns $\mathbf{b}_1, \dots, \mathbf{b}_N$.

Thus every convex polygon Δ in \mathbb{R}^2 with vertices in \mathbb{Z}^2 and non-empty interior can be viewed as the secondary polygon of some rank 2 subgroup $\mathbb{L} \subset \mathbb{Z}^N$ satisfying the conditions in 2.1.

Note however that in general there are several possible choices for the points $\mathbf{p}_1, \dots, \mathbf{p}_N$ in $\partial\Delta \cap \mathbb{Z}^2$. The minimal choice takes only the vertices of Δ , while the maximal choice takes all points of $\partial\Delta \cap \mathbb{Z}^2$.

3.9. Theorem. *The (Euclidean) area of the polygon Δ in (8) is*

$$\text{area } \Delta = \frac{1}{2} \sum_{1 \leq i < j \leq N} |\det(\mathbf{b}_i, \mathbf{b}_j)| - \sum_{\{i,j\} \in L_C} |\det(\mathbf{b}_i, \mathbf{b}_j)| \quad (9)$$

for every 2-dimensional cone C in the secondary fan.

Proof. After applying, if necessary, a cyclic permutation to $\mathbf{b}_1, \dots, \mathbf{b}_N$ we may assume, without loss of generality, that $C = \mathbb{R}_{\geq 0}\mathbf{b}_1 + \mathbb{R}_{\geq 0}\mathbf{b}_N$.

From the triangulation Δ by the diagonals between the vertex $\mathbf{p}_N = \mathbf{0}$ and the other vertices of Δ one sees that $\text{area } \Delta = \frac{1}{2} \sum_{1 \leq i < j \leq M} \det(\mathbf{b}_i, \mathbf{b}_j)$ where M is such that $\mathbf{b}_j \notin \mathbb{R}_{\geq 0}\mathbf{b}_N$ for $1 \leq j \leq M$ and $\mathbf{b}_j \in \mathbb{R}_{\geq 0}\mathbf{b}_N$ for $M+1 \leq j \leq N$. The fact that $\sum_{i=1}^N \mathbf{b}_i = \mathbf{0}$, implies

$$\sum_{1 \leq i \leq M < j \leq N} \det(\mathbf{b}_i, \mathbf{b}_j) = \det(\sum_{1 \leq i \leq M} \mathbf{b}_i, \sum_{M < j \leq N} \mathbf{b}_j) = 0.$$

Thus we see

$$\text{area } \Delta = \frac{1}{2} \sum_{1 \leq i < j \leq N} \det(\mathbf{b}_i, \mathbf{b}_j).$$

Next note that for $1 \leq i < j \leq N$ the inequality $\det(\mathbf{b}_i, \mathbf{b}_j) < 0$ holds if and only if $C \subset \mathbb{R}_{\geq 0}\mathbf{b}_i + \mathbb{R}_{\geq 0}\mathbf{b}_j$, if and only if $\{i, j\} \in L_C$. Equality (9) now follows immediately. \blacksquare

3.10. Corollary. *The number of lattice points in the interior of the polygon Δ in (8) is*

$$\frac{1}{2} \left(\sum_{1 \leq i < j \leq N} |\det(\mathbf{b}_i, \mathbf{b}_j)| - N \right) - \sum_{\{i,j\} \in L_C} |\det(\mathbf{b}_i, \mathbf{b}_j)| + 1.$$

Proof. This follows from Theorem 3.9 in combination with *Pick's Formula* ([7] p.113): $2\text{area } \Delta = 2\sharp(\mathbb{Z}^2 \cap \text{interior } \Delta) + \sharp(\mathbb{Z}^2 \cap \text{boundary } \Delta) - 2$ \blacksquare

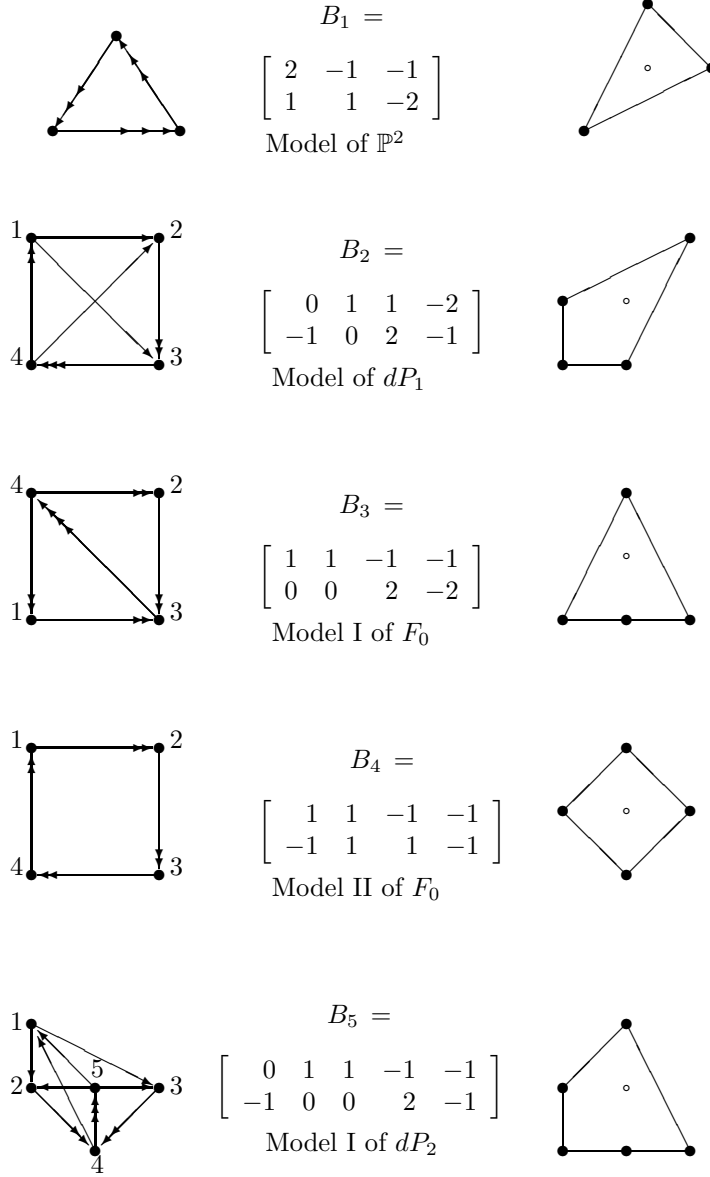


Figure 3: *Quivers from [3] Figures 10, 11, 4, 12 and corresponding polygons.*

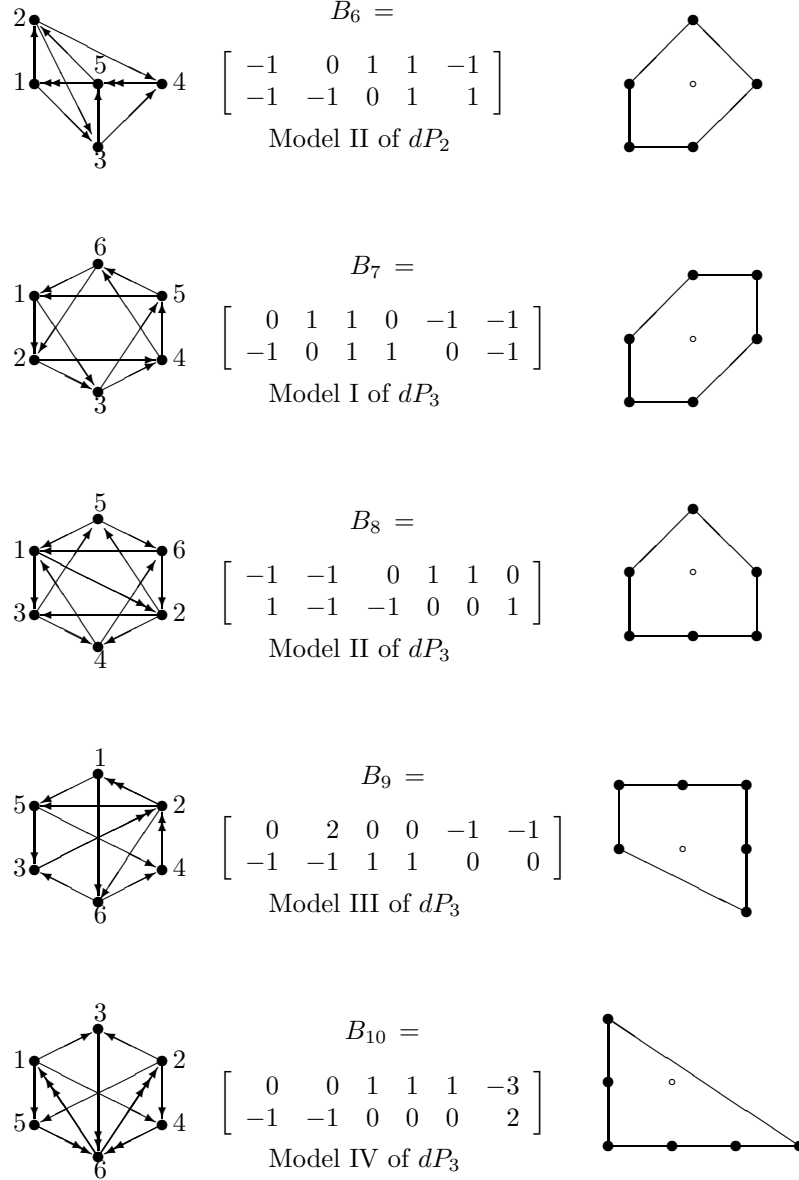


Figure 4: Quivers from [3] Figures 12, 9 and corresponding polygons.

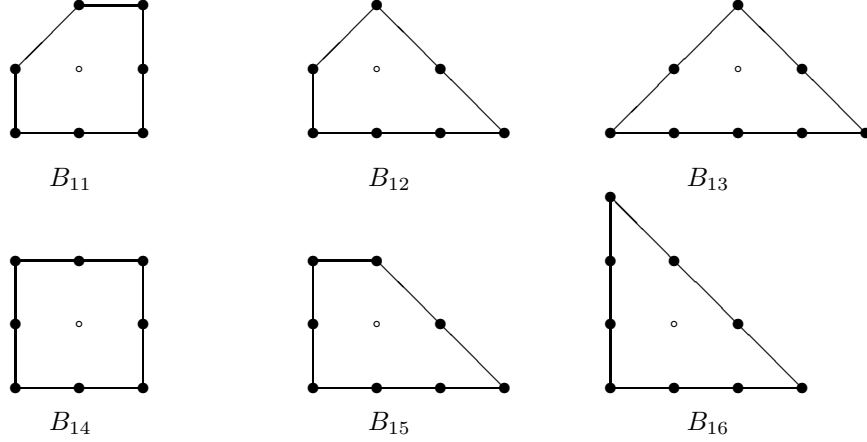


Figure 5: *Remaining reflexive polygons.*

3.11. Example. Figures 3 and 4 show some examples of the above relation between quivers, rank 2 subgroups \mathbb{L} of \mathbb{Z}^N as in 2.1 and polygons. The quivers are taken from [3]. We name our examples neutrally as B_1, \dots, B_{10} , but also mention the names given to these quiver models in [3]. The latter names refer to del Pezzo surfaces dP_k , i.e. the projective plane \mathbb{P}^2 blown up in k points, some of which, on the present occasion, may happen to be “infinitely near” and therefore require repeated blow-ups. With the latter somewhat liberal use of the name *del Pezzo surface*, dP_k matches well with the toric geometry of the fan whose 1-dimensional rays are the half-lines from the interior lattice point \circ through a lattice point \bullet at the boundary. Note however that this fan is in general not the same as the secondary fan and that therefore the singularity associated with the polygon (cf. [12, 19]) is not the singularity obtained by contracting to a point the zero-section of the canonical bundle of the del Pezzo surface.

The polygons in Figures 3 and 4, however, are in general different from, the polygons associated with the same quiver in [3] Figure 8. We will clarify this issue in 6.14, 6.15, 6.16.

It is remarkable that the polygons in Figures 3 and 4 are exactly the lattice polygons with one interior lattice point and ≤ 6 lattice points on the boundary. There are exactly 16 lattice polygons with one interior lattice point. The remaining 6 are shown in Figure 5. A nice review of these so-called *reflexive polygons* can be found in [21].

In cases B_1 , B_3 and B_4 the greatest common divisor d of the entries in the quiver’s adjacency matrix is > 1 and the polygon in these cases depends

on an integer matrix with determinant d . We have chosen this matrix such that the polygon is a reflexive polygon.

4 GKZ hypergeometric systems

4.1. In the late 1980's Gelfand, Kapranov and Zelevinsky discovered fascinating generalizations of the classical hypergeometric structures of Euler, Gauss, Appell, Lauricella, Horn [8, 9, 10, 11, 25]. The main ingredient for these new hypergeometric structures is a finite sequence $\mathcal{A} = (\mathbf{a}_1, \dots, \mathbf{a}_N)$ of vectors in \mathbb{Z}^{k+1} which generates \mathbb{Z}^{k+1} as an abelian group and for which there exists a group homomorphism $h : \mathbb{Z}^{k+1} \rightarrow \mathbb{Z}$ such that $h(\mathbf{a}_i) = 1$ for all i . The latter condition means that \mathcal{A} lies in a k -dimensional affine hyperplane in \mathbb{Z}^{k+1} . Figure 6 shows \mathcal{A} (each black dot represents one vector) sitting in this hyperplane for some classical hypergeometric structures. Gelfand, Kapranov and Zelevinsky called these new structures *\mathcal{A} -hypergeometric systems*, but nowadays most authors call them *GKZ hypergeometric systems*.

Let \mathbb{L} denote the lattice (= free abelian group) of linear relations in \mathcal{A} :

$$\mathbb{L} := \{(\ell_1, \dots, \ell_N) \in \mathbb{Z}^N \mid \ell_1 \mathbf{a}_1 + \dots + \ell_N \mathbf{a}_N = \mathbf{0}\}. \quad (10)$$

It follows from the above construction and assumptions that the quotient group $\mathbb{Z}^N / \mathbb{L}$ is \mathbb{Z}^{k+1} , and a fortiori, it is torsion free.

In this paper we consider only the case when the rank of \mathbb{L} is 2; i.e. $k+1 = N-2$. Since we assumed the existence of a linear map $h : \mathbb{Z}^{N-2} \rightarrow \mathbb{Z}$ such that $h(\mathbf{a}_i) = 1$ for all i , \mathbb{L} lies in the kernel of the map \mathbf{s} defined by:

$$\mathbf{s} : \mathbb{R}^N \rightarrow \mathbb{R}, \quad \mathbf{s}(z_1, \dots, z_N) = z_1 + \dots + z_N. \quad (11)$$

The following lemma shows what the other condition for \mathbb{L} in 2.1 means in terms of \mathcal{A} .

4.2. Proposition. *In the situation of 4.1 the following statements are equivalent:*

1. \mathbb{L} is not contained in any of the standard coordinate hyperplanes of \mathbb{Z}^N .
2. No vector in the sequence \mathcal{A} is linearly independent of the other vectors.
3. For every i the lattice of linear relations between the vectors of $\mathcal{A} \setminus \{\mathbf{a}_i\}$ has rank 1.

Proof. Assume \mathbb{L} is contained in the i -th coordinate hyperplane. Then the i -th component of every element of \mathbb{L} is 0 and hence \mathbf{a}_i occurs in no linear relation for the vectors in \mathcal{A} . In other words, \mathbb{L} is the lattice of linear

relations between the vectors of $\mathcal{A} \setminus \{\mathbf{a}_i\}$. Since \mathbb{L} has rank 2, we conclude that statement 3 implies statement 1.

Conversely, assume that the lattice \mathbb{L}_i of linear relations between the vectors of $\mathcal{A} \setminus \{\mathbf{a}_i\}$ has rank > 1 . Since \mathbb{L}_i is contained in \mathbb{L} and the latter has rank 2, we see that $\mathbb{L}_i \otimes \mathbb{R} = \mathbb{L} \otimes \mathbb{R}$. Therefore, since \mathbb{L}_i is contained in the i -th coordinate hyperplane, so is \mathbb{L} . Hence statement 1 implies statement 3.

It is obvious that statements 1 and 2 are equivalent. \blacksquare

4.3. Definition. A subsequence \mathcal{A}' of \mathcal{A} is said to be *minimally dependent* if the vectors in \mathcal{A}' are linearly dependent and the vectors in every subsequence \mathcal{A}'' of \mathcal{A}' with $\mathcal{A}'' \neq \mathcal{A}'$ are linearly independent. A linear dependence relation $\sum_j \alpha_j \mathbf{a}_j = 0$ is a *minimal linear dependence relation* in \mathcal{A} if the subsequence $(\mathbf{a}_j \mid \alpha_j \neq 0)$ is minimally dependent.

4.4. Proposition.

1. Let B be a $2 \times N$ -matrix such that its rows are a \mathbb{Z} -basis for \mathbb{L} . Let $\mathbf{b}_1, \dots, \mathbf{b}_N$ be the columns of this matrix. Then one has for every i

$$\sum_{j=1}^N \det(\mathbf{b}_i, \mathbf{b}_j) \mathbf{a}_j = \mathbf{0}. \quad (12)$$

2. Assume the conditions in Proposition 4.2 are satisfied. Then every linear relation (12) is minimal and every minimal linear dependence relation in \mathcal{A} is a non-zero scalar multiple of some relation (12).

Proof. For statement 1, let A be the matrix with columns $\mathbf{a}_1, \dots, \mathbf{a}_N$. Then Equation (10) can be rewritten as $BA^t = 0$. This implies $B^t JBA^t = 0$, which is just a compressed form of the relations we wanted to prove.

For statement 2 note that condition 3 in Proposition 4.2 implies that every linear relation (12) is minimal. Conversely, consider a minimal linear relation $\sum_j \alpha_j \mathbf{a}_j = 0$. Then the subsequence $(\mathbf{a}_j \mid \alpha_j \neq 0)$ has at most $N - 1$ elements. The given minimal relation is therefore a non-zero scalar multiple of at least one relation (12). \blacksquare

4.5. Gelfand, Kapranov and Zelevinsky [8, 9, 10] associate with a set \mathcal{A} as in 4.1 and a vector $\mathbf{c} \in \mathbb{C}^{k+1}$ the following system of partial differential equations for functions Φ of N variables u_1, \dots, u_N :

- for every $(\ell_1, \dots, \ell_N) \in \mathbb{L}$ one differential equation

$$\prod_{\ell_i < 0} \left(\frac{\partial}{\partial u_i} \right)^{-\ell_i} \Phi = \prod_{\ell_i > 0} \left(\frac{\partial}{\partial u_i} \right)^{\ell_i} \Phi, \quad (13)$$

- the system of $k + 1$ differential equations

$$\mathbf{a}_1 u_1 \frac{\partial \Phi}{\partial u_1} + \dots + \mathbf{a}_N u_N \frac{\partial \Phi}{\partial u_N} = \mathbf{c} \Phi. \quad (14)$$

4.6. Example. The sequence $\mathcal{A} = (\mathbf{a}_1, \mathbf{a}_2, \mathbf{a}_3, \mathbf{a}_4) \in \mathbb{Z}^2$ for Example B_2 in Figure 3 can be taken to be

$$\mathbf{a}_1 = \begin{bmatrix} 1 \\ 0 \end{bmatrix}, \quad \mathbf{a}_3 = \begin{bmatrix} 1 \\ 1 \end{bmatrix}, \quad \mathbf{a}_4 = \begin{bmatrix} 1 \\ 2 \end{bmatrix}, \quad \mathbf{a}_2 = \begin{bmatrix} 1 \\ 3 \end{bmatrix}.$$

It is a classical result of K. Mayr that the roots of the 1-variable cubic polynomial $P(x) = u_1 + u_3x + u_4x^2 + u_2x^3$ as functions of the coefficients u_1, \dots, u_4 satisfy the GKZ system of differential equations for this \mathcal{A} and with $\mathbf{c} = \begin{bmatrix} 0 \\ -1 \end{bmatrix}$; see e.g. [25] §2.1.

4.7. Example. An important example in the toric geometry constructions of Sasaki-Einstein manifolds is known under the name $L^{a,b,c}$; see e.g. [6]. Here a, b, c are integers with $c \leq b$ and $0 < a \leq b$. The polygon for this example, displayed in [6] Figure 2, is a quadrangle with vertices $(0, 0)$, $(1, 0)$, (ak, b) , $(-al, c)$ where k and l are integers such that $ck + bl = 1$. The method explained in 3.8 yields $\mathbb{L} = \mathbb{Z}(1, ak - 1, -al - ak, al) \oplus \mathbb{Z}(0, b, c - b, -c)$. From this we see that we can take $\mathcal{A} = (\mathbf{a}_1, \mathbf{a}_2, \mathbf{a}_3, \mathbf{a}_4) \in \mathbb{Z}^2$ with

$$\mathbf{a}_1 = \begin{bmatrix} 1 \\ c - a \end{bmatrix}, \quad \mathbf{a}_2 = \begin{bmatrix} 1 \\ c \end{bmatrix}, \quad \mathbf{a}_3 = \begin{bmatrix} 1 \\ 0 \end{bmatrix}, \quad \mathbf{a}_4 = \begin{bmatrix} 1 \\ b \end{bmatrix}.$$

As in Example 4.6 this means that the corresponding GKZ system deals with the roots of the “four-nomial” $u_1x^{c-a} + u_2x^c + u_3 + u_4x^b$ as functions of the coefficients u_1, u_2, u_3, u_4 .

According to [6] §3 the examples $Y^{p,q}$ of [1, 19] are special cases of the above: $Y^{p,q} = L^{p-q, p+q, p}$. So, these correspond to the “four-nomials” $u_1x^q + u_2x^p + u_3 + u_4x^{p+q}$. Thus Example 4.6 is in fact $Y^{2,1} = L^{1,3,2}$.

4.8. Example. From the pictures of \mathcal{A} shown in Figure 6 one easily sees that for the Gauss system the lattice \mathbb{L} is generated by the vector $(1, 1, -1, -1)$ and thus has rank 1 and is not of interest here. For Appell’s F_1 and F_4 the lattice \mathbb{L} has rank 2 and the corresponding B -matrices are

$$F_1 : \begin{bmatrix} 1 & -1 & 0 & -1 & 1 & 0 \\ 1 & 0 & -1 & -1 & 0 & 1 \end{bmatrix}, \quad F_4 : \begin{bmatrix} -1 & -1 & 1 & 1 & 0 & 0 \\ -1 & -1 & 0 & 0 & 1 & 1 \end{bmatrix}.$$

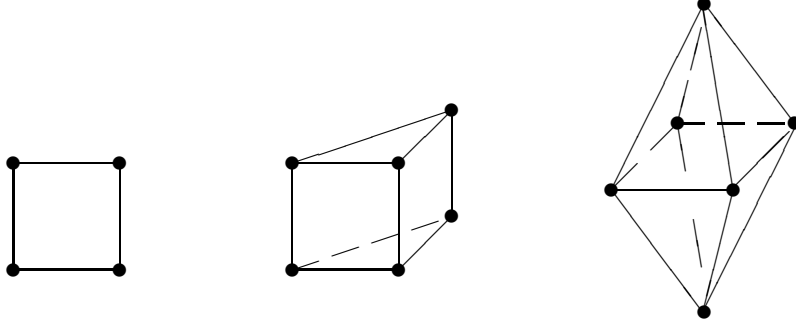
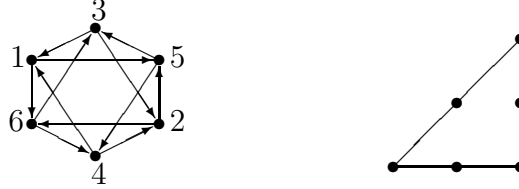


Figure 6: *The sets \mathcal{A} for Gauss's hypergeometric functions (left), Appell's F_1 (middle) and Appell's F_4 (right).*

Thus Appell's F_1 corresponds to B_7 in Figure 4. For Appell's F_4 the quiver and the polygon are



In [8] §3.2 Gelfand, Kapranov and Zelevinsky discuss how the 14 complete hypergeometric Horn series in two variables fit their theory. It is an amusing simple exercise to now find the corresponding quivers and polygons. It turns out that, with the exception of F_4 , all Horn series give a quiver listed in Example 3.11:

$$\begin{aligned} \{G_3\} &\leftrightarrow B_2, & \{H_5\} &\leftrightarrow B_5, & \{G_1, H_3, H_6\} &\leftrightarrow B_6, & \{F_1, G_2\} &\leftrightarrow B_7, \\ \{H_1\} &\leftrightarrow B_8, & \{H_4, H_7\} &\leftrightarrow B_9, & \{F_2, F_3, H_2\} &\leftrightarrow B_{11}. \end{aligned}$$

4.9. In 4.1 we started from the sequence of vectors \mathcal{A} and then defined \mathbb{L} via Equation (10). Let us reverse the procedure and start with a rank 2 subgroup $\mathbb{L} \subset \mathbb{Z}^N$ as in 2.1. We can now define

$$\begin{aligned} \mathcal{A} &= (\mathbf{a}_1, \dots, \mathbf{a}_N) \quad \text{with} \\ \mathbf{a}_i &= \text{the class } \mathbf{e}_i \text{ mod } \mathbb{L} \text{ in the quotient group } \mathbb{Z}^N/\mathbb{L}. \end{aligned} \tag{15}$$

If the quotient group \mathbb{Z}^N/\mathbb{L} is torsion free, it is isomorphic to \mathbb{Z}^{N-2} and the sequence of vectors \mathcal{A} in (15) satisfies the requirements of 4.1. *Thus (10) and (15) give equivalences, inverse to each other, between the data \mathcal{A} and \mathbb{L} .*

In combination with Theorem 2.10 this gives

4.10. Theorem. *There is an equivalence of data between on the one hand sequences \mathcal{A} as in 4.1 which satisfy also the conditions in Proposition 4.2 and*

on the other hand quivers without isolated nodes or directed loops of length ≤ 2 , such that in every node the number of incoming arrows equals the number of outgoing arrows and such that for its anti-symmetrized adjacency matrix the rank is 2 and the greatest common divisor of the entries is 1. ■

4.11. Remark. We refer to 5.5 for a discussion of how to extend the definition of GKZ systems so as to allow for torsion in the group \mathbb{Z}^N/\mathbb{L} .

4.12. In order to have an efficient method to construct bases for the solution space of the hypergeometric system (13)-(14) Gelfand, Kapranov and Zelevinsky developed the theory of the *secondary fan* and the *secondary polytope*. The term “secondary” refers to the habit of considering the set \mathcal{A} as primary data and to call the convex hull of \mathcal{A} the *primary polytope*.

In case the lattice \mathbb{L} of relations in \mathcal{A} has rank 2, the constructions become particularly simple. The secondary fan is the one in Definition 3.2. With a 2-dimensional cone C in the secondary fan one associates a set L_C of 2-element subsets of $\{1, \dots, N\}$ as in Equation (4). One can interpret this L_C as a triangulation of the primary polytope $\text{convex hull}(\mathcal{A})$ as follows. Recall that $\mathcal{A} = (\mathbf{a}_1, \dots, \mathbf{a}_N)$ and assume for convenience of imagining pictures that all \mathbf{a}_i ’s are different. For $\{i, j\} \in L_C$ set $T_{\{i,j\}} := \text{convex hull}(\{\mathbf{a}_k \mid k \neq i, j\})$. This $T_{\{i,j\}}$ is an $(N-3)$ -dimensional simplex and the simplices $T_{\{i,j\}}$ with $\{i, j\} \in L_C$ together constitute a *triangulation the primary polytope*.

In [11] p.220 the *secondary polytope* is constructed (and defined) in terms of these triangulations as follows. For a 2-element subset $\{i, j\} \subset \{1, \dots, N\}$ with $i < j$ let A_{ij} denote the $(N-2) \times (N-2)$ -matrix with columns \mathbf{a}_k for $k \neq i, j$ in the natural order of increasing indices. To a 2-dimensional cone C in the secondary fan one then associates the vector

$$\varphi_C := \sum_{\{i,j\} \in L_C} |\det A_{ij}| \sum_{k \neq i,j} \mathbf{e}_k. \quad (16)$$

Then in [11] p.220 the *secondary polytope* $\Sigma(\mathcal{A})$ is defined as

$$\Sigma(\mathcal{A}) := \text{convex hull}(\{\varphi_C \mid C \text{ 2-dim cone of secondary fan}\}). \quad (17)$$

As $|\det A_{ij}|$ is $(N-3)!$ times the Euclidean volume of the simplex $T_{\{i,j\}}$, the number $\text{vol}_{\mathcal{A}} := \sum_{\{i,j\} \in L_C} |\det A_{ij}|$ is for every C equal to $(N-3)!$ times the Euclidean volume of the primary polytope $\text{convex hull}(\mathcal{A})$ and the point

$$\frac{1}{(N-2)\text{vol}_{\mathcal{A}}} \sum_{\{i,j\} \in L_C} |\det A_{ij}| \sum_{k \neq i,j} \mathbf{a}_k$$

coincides for every C with the barycentre of the primary polytope. The secondary polytope therefore lies in a 2-dimensional plane parallel to $\mathbb{L}_{\mathbb{R}}$.

4.13. Let us compare $\Sigma(\mathcal{A})$ with the polytope $\Sigma(\mathbb{L})$ of Definition 3.3. It is a well-known and easy to prove fact that $|\det A_{ij}| = |\det(\mathbf{b}_i, \mathbf{b}_j)|$ for all $\{i, j\} \in L_C$ (see e.g. [25] Eq. (62)). Thus Equations (16) and (5) yield

$$\varphi_C = -\psi_C + \text{vol}_{\mathcal{A}} \cdot \sum_{k=1}^N \mathbf{e}_k, \quad (18)$$

with

$$\text{vol}_{\mathcal{A}} = \sum_{\{i,j\} \in L_C} |\det A_{ij}| = \sum_{\{i,j\} \in L_C} |\det(\mathbf{b}_i, \mathbf{b}_j)|. \quad (19)$$

This means that the two secondary polytopes $\Sigma(\mathcal{A})$ and $\Sigma(\mathbb{L})$ are related by a point symmetry with centre $\frac{1}{2}\text{vol}_{\mathcal{A}} \cdot \sum_{k=1}^N \mathbf{e}_k$:

$$\Sigma(\mathcal{A}) = -\Sigma(\mathbb{L}) + \text{vol}_{\mathcal{A}} \cdot \sum_{k=1}^N \mathbf{e}_k. \quad (20)$$

5 About the solutions to GKZ systems.

5.1. The variables in GKZ theory (see Section 4) are the natural coordinates on the space $\mathbb{C}^{\mathcal{A}} := \text{Maps}(\mathcal{A}, \mathbb{C})$ of maps from \mathcal{A} to \mathbb{C} . The torus $\mathbb{T}^{k+1} := \text{Hom}(\mathbb{Z}^{k+1}, \mathbb{C}^*)$ of group homomorphisms from \mathbb{Z}^{k+1} to \mathbb{C}^* , acts naturally on $\mathbb{C}^{\mathcal{A}}$ and on the functions on this space: for $\sigma \in \mathbb{T}^{k+1}$, $\mathbf{u} \in \mathbb{C}^{\mathcal{A}}$, $\mathbf{a} \in \mathcal{A}$ and $\Phi : \mathbb{C}^{\mathcal{A}} \rightarrow \mathbb{C}$:

$$(\sigma \cdot \mathbf{u})(\mathbf{a}) = \sigma(\mathbf{a})\mathbf{u}(\mathbf{a}), \quad (\Phi \cdot \sigma)(\mathbf{u}) = \Phi(\sigma \cdot \mathbf{u}). \quad (21)$$

The GKZ hypergeometric functions associated with \mathcal{A} and \mathbf{c} are defined on open domains in $\mathbb{C}^{\mathcal{A}}$. One easily sees that if a function Φ on $\mathbb{C}^{\mathcal{A}}$ satisfies the differential equations (13) then for every $\sigma \in \mathbb{T}^{k+1}$ the function $\Phi \cdot \sigma$ also satisfies these differential equations. So, the torus \mathbb{T}^{k+1} acts on the solution space of the system of differential equations (13).

On the other hand, if Φ_1 and Φ_2 are two functions which satisfy the differential equations (14) with the same \mathbf{c} , then their quotient $\Psi = \frac{\Phi_1}{\Phi_2}$ satisfies

$$\mathbf{a}_1 u_1 \frac{\partial \Psi}{\partial u_1} + \dots + \mathbf{a}_N u_N \frac{\partial \Psi}{\partial u_N} = \mathbf{0}.$$

The latter equation is equivalent to Ψ being \mathbb{T}^{k+1} -invariant. Thus we find:

All quotients of pairs of solutions of the system (13)-(14) are functions on simply connected open subsets of the orbit space $\mathbb{C}^{\mathcal{A}}/\mathbb{T}^{k+1}$. In the case of interest in the present paper the dimension of this orbit space is $N - k - 1 = 2$.

For $\mathbf{c} \in \mathbb{Z}^{k+1}$ the differential equations (14) are equivalent with Φ transforming under the action of \mathbb{T}^{k+1} according to the character given by \mathbf{c} :

$$\Phi \cdot \sigma = \sigma(\mathbf{c})\Phi. \quad (22)$$

In particular for $\mathbf{c} = \mathbf{0}$ all solutions of (14) are \mathbb{T}^{k+1} -invariant.

5.2. The space $(\mathbb{C}^*)^{\mathcal{A}} := \text{Maps}(\mathcal{A}, \mathbb{C}^*)$ of maps from \mathcal{A} to \mathbb{C}^* is a torus of dimension N which contains \mathbb{T}^{k+1} as a subtorus. The action (21) of $\sigma \in \mathbb{T}^{k+1}$ on $\mathbb{C}^{\mathcal{A}}$ obviously restricts to the action of \mathbb{T}^{k+1} on $(\mathbb{C}^*)^{\mathcal{A}}$ by multiplication. The quotient space $(\mathbb{C}^*)^{\mathcal{A}}/\mathbb{T}^{k+1}$, which is a subspace of $\mathbb{C}^{\mathcal{A}}/\mathbb{T}^{k+1}$, is the torus $\text{Hom}(\mathbb{L}, \mathbb{C}^*)$ of group homomorphisms from \mathbb{L} to \mathbb{C}^* . The toric variety associated with the secondary fan (cf. Definition 3.2) gives a compactification of the torus $\text{Hom}(\mathbb{L}, \mathbb{C}^*)$; see [7] for the general theory of toric varieties. It is an essential part of the GKZ philosophy that quotients of hypergeometric functions should be viewed as being defined on open subsets of this toric variety.

5.3. Theorem. (cf. [8] Theorems 2 and 5, [8]', [26] Prop. 13.5) *Let*

$$\begin{aligned} \mathbb{N}\mathcal{A} &= \{x_1\mathbf{a}_1 + \dots + x_N\mathbf{a}_N \in \mathbb{R}^{k+1} \mid \forall x_i \in \mathbb{Z}_{\geq 0}\}, \\ \mathbb{Z}\mathcal{A} &= \{x_1\mathbf{a}_1 + \dots + x_N\mathbf{a}_N \in \mathbb{R}^{k+1} \mid \forall x_i \in \mathbb{Z}\}, \\ \text{pos}(\mathcal{A}) &= \{x_1\mathbf{a}_1 + \dots + x_N\mathbf{a}_N \in \mathbb{R}^{k+1} \mid \forall x_i \in \mathbb{R}_{\geq 0}\}. \end{aligned}$$

Assume $\mathbb{N}\mathcal{A} = \mathbb{Z}\mathcal{A} \cap \text{pos}(\mathcal{A})$, then the dimension of the space of solutions of the system of differential equations (13)-(14) at a general point of $\mathbb{C}^{\mathcal{A}}$ equals the number $\text{vol}_{\mathcal{A}}$ in Equation (19). ■

5.4. Remark. As shown in the proof of [26] Prop. 13.15 the condition $\mathbb{N}\mathcal{A} = \mathbb{Z}\mathcal{A} \cap \text{pos}(\mathcal{A})$ in the above theorem is satisfied if \mathcal{A} admits a *unimodular triangulation*. The latter condition is equivalent to: there is a cone C in the secondary fan such that $|\det(\mathbf{b}_i, \mathbf{b}_j)| = 1$ for all $\{i, j\} \in L_C$ (see Definitions 3.2 and 3.3).

5.5. Remark. From the discussion in 5.1 one may get an idea about extending the GKZ system (13)-(14) to the situation in which \mathbb{Z}^N/\mathbb{L} has a non-trivial torsion subgroup $(\mathbb{Z}^N/\mathbb{L})_{\text{tors}}$. Equation (13) still makes sense in this more general situation, but Equation (14) must be adapted.

Recall from (15) a definition of \mathcal{A} which also works in the torsion case. Let $\mathcal{G}_{\mathcal{A}} := \text{Hom}(\mathbb{Z}^N/\mathbb{L}, \mathbb{C}^*)$. This is a commutative algebraic group of which the connected component of the identity is $\mathcal{G}_{\mathcal{A}}^{\circ} = \mathbb{T}^{k+1} = \text{Hom}(\mathbb{Z}^{k+1}, \mathbb{C}^*)$ and the group of connected components is the finite abelian group $\mathcal{G}_{\mathcal{A}}/\mathcal{G}_{\mathcal{A}}^{\circ} = \text{Hom}((\mathbb{Z}^N/\mathbb{L})_{\text{tors}}, \mathbb{C}^*) \simeq (\mathbb{Z}^N/\mathbb{L})_{\text{tors}}$. Formula (21) defines an action of $\mathcal{G}_{\mathcal{A}}$ on

\mathbb{C}^A and on the functions on \mathbb{C}^A . It is now clear how to adapt Equation (14): let $\bar{\mathbf{a}}_i$ denote the projection of \mathbf{a}_i in the free part \mathbb{Z}^{k+1} of \mathbb{Z}^N/\mathbb{L} and replace (14) by

$$\bar{\mathbf{a}}_1 u_1 \frac{\partial \Phi}{\partial u_1} + \dots + \bar{\mathbf{a}}_N u_N \frac{\partial \Phi}{\partial u_N} = \mathbf{c} \Phi$$

plus the requirement that the solution should transform according to some character of the finite abelian group $(\mathbb{Z}^N/\mathbb{L})_{\text{tors}}$.

5.6. Example. In case B_1 in Figure 3 one has $\mathbb{L} = \mathbb{Z}(2, -1, -1) \oplus \mathbb{Z}(1, 1, -2)$ and $\mathbb{Z}^3/\mathbb{L} = \mathbb{Z} \oplus \mathbb{Z}/3\mathbb{Z}$. As a generator for the torsion subgroup we take $\mathbf{g} = (1, -1, 0) \bmod \mathbb{L}$. Then the polynomials $\Phi_0 = \frac{1}{2}u_3^2 + u_1u_2$, $\Phi_1 = \frac{1}{2}u_2^2 + u_1u_3$ and $\Phi_2 = \frac{1}{2}u_1^2 + u_2u_3$ satisfy the differential equations (13) for \mathbb{L} , the differential equations (14) for $\mathbf{c} = 2$, while $\mathbf{g} \cdot \Phi_r = e^{2\pi i r/3} \Phi_r$ for $r = 0, 1, 2$.

6 From rank 2 subgroups of \mathbb{Z}^N to Dessins.

We are going to describe a construction which associates with a rank 2 subgroup \mathbb{L} of \mathbb{Z}^N , as in 2.1, *dessins d'enfants*, i.e. bipartite graphs embedded in oriented Riemann surfaces.

The construction is given in [14] §5 and §6 as *Fast Inverse Algorithm*. In op. cit., however, this algorithm is only presented via explicit visual inspection of pictures in some concrete examples. In this section we want to present a general principle behind the Fast Inverse Algorithm of [14] which uses only linear algebra and can be performed by computer.

The main part of our construction produces rhombus tilings of the plane and is the same as N.G. de Bruijn's [2] construction of Penrose tilings. His work also led to effective methods for making *quasi-crystals* [23]. Since \mathbb{L} is defined over \mathbb{Z} the construction yields in our situation periodic tilings of the plane $\mathbb{L}_{\mathbb{R}}^{\vee} = \mathbb{R}^2$, not just quasi-periodic ones. We can therefore pass to \mathbb{R}^2 modulo the period lattice and find a tiling of the two-dimensional torus.

6.1. In this section \mathbb{L} is as in 2.1. The quotient group \mathbb{Z}^N/\mathbb{L} is allowed to have torsion. Let $\mathbb{L}_{\mathbb{R}}$ denote the real 2-plane in \mathbb{R}^N which contains \mathbb{L} . We write $\lambda + \mathbb{L}_{\mathbb{R}}$ for the real 2-plane in \mathbb{R}^N obtained by translating $\mathbb{L}_{\mathbb{R}}$ over a vector $\lambda \in \mathbb{R}^N$. On the other hand one has in \mathbb{R}^N the *standard N -grid* consisting of the hyperplanes

$$\mathcal{H}_{i,k} := \{(z_1, \dots, z_N) \in \mathbb{R}^N \mid z_i = k\} \quad \text{for } i = 1, \dots, N \text{ and } k \in \mathbb{Z}.$$

By intersecting with this standard N -grid we obtain in the 2-plane $\lambda + \mathbb{L}_{\mathbb{R}}$ an N -grid of lines:

$$\mathcal{L}_{i,k}^{\lambda} := \mathcal{H}_{i,k} \cap (\lambda + \mathbb{L}_{\mathbb{R}}) \quad \text{for } i = 1, \dots, N \text{ and } k \in \mathbb{Z}. \quad (23)$$

Note that this crucially uses the assumption that \mathbb{L} is not contained in any of the standard coordinate hyperplanes in \mathbb{Z}^N .

The grid lines are naturally oriented: the orientation on $\mathcal{L}_{i,k}^\lambda$ is such that the points in $\lambda + \mathbb{L}_\mathbb{R}$ which are to the left of $\mathcal{L}_{i,k}^\lambda$, have a larger i -th coordinate than the points to the right of $\mathcal{L}_{i,k}^\lambda$.

6.2. Definition. We say that λ is *non-resonant* if no three grid lines pass through one point.

6.3. First step. Let \mathbb{L} and λ be as in 6.1 with λ non-resonant as in 6.2. Consider the map

$$F : \mathbb{R}^N \rightarrow \mathbb{Z}^N, \quad F(z_1, \dots, z_N) = (\lfloor z_1 \rfloor, \dots, \lfloor z_N \rfloor),$$

where $\lfloor z \rfloor$ for a real number z denotes the largest integer $\leq z$. The map F contracts an open N -cube in the \mathbb{Z}^N structure on \mathbb{R}^N (and part of its boundary) onto one of its corners. F commutes with the translation action of \mathbb{Z}^N on \mathbb{R}^N and \mathbb{Z}^N . Suppressing \mathbb{L} and λ from the notation we define

$$\mathcal{S}^0 := F(\lambda + \mathbb{L}_\mathbb{R}). \quad (24)$$

The map F is constant on each 2-cell (= connected component) of the grid complement in $\lambda + \mathbb{L}_\mathbb{R}$. Every point of \mathcal{S}^0 is in fact the image of a unique such 2-cell. The distance between two points of \mathcal{S}^0 is 1 if and only if the corresponding 2-cells are separated by exactly one grid line.

Because λ is non-resonant, an intersection point of grid lines is in the closure of exactly four 2-cells. If $\mathbf{x} = \mathcal{L}_{i,k}^\lambda \cap \mathcal{L}_{j,m}^\lambda$ the four points of \mathcal{S}^0 corresponding to these cells, i.e. $F(\mathbf{x})$, $F(\mathbf{x}) - \mathbf{e}_i$, $F(\mathbf{x}) - \mathbf{e}_j$, $F(\mathbf{x}) - \mathbf{e}_i - \mathbf{e}_j$, are the vertices of a square $\square_{\mathbf{x}}$. When \mathbf{x} runs through the set of all intersection points of grid lines, these squares fit together to a connected surface $\mathcal{S} := \bigcup_{\mathbf{x}} \square_{\mathbf{x}}$ embedded in \mathbb{R}^N . One can characterize the surface \mathcal{S} also as

$$\mathcal{S} := \text{union of all unit squares in } \mathbb{R}^N \text{ with vertices in the set } \mathcal{S}^0. \quad (25)$$

Here one may define *unit square* as the convex hull of four points $\mathbf{p}_1, \mathbf{p}_2, \mathbf{p}_3, \mathbf{p}_4$ in \mathbb{R}^N with Euclidean distances $\|\mathbf{p}_1 - \mathbf{p}_2\| = \|\mathbf{p}_2 - \mathbf{p}_3\| = \|\mathbf{p}_3 - \mathbf{p}_4\| = \|\mathbf{p}_4 - \mathbf{p}_1\| = 1$ and $\|\mathbf{p}_1 - \mathbf{p}_3\| = \|\mathbf{p}_2 - \mathbf{p}_4\| = \sqrt{2}$. A unit square with vertices in \mathbb{Z}^N is necessarily of the form $\mathbf{p} + \text{convex hull}(\mathbf{0}, \mathbf{e}_i, \mathbf{e}_j, \mathbf{e}_i + \mathbf{e}_j)$ for some $\mathbf{p} \in \mathbb{Z}^N$ and some i, j . We say that a unit square in \mathbb{R}^N has *type* (i, j) if its sides are parallel to the vectors \mathbf{e}_i or \mathbf{e}_j . Similarly, a side of a unit square in \mathbb{R}^N has *type* i if it is parallel to the vector \mathbf{e}_i .

6.4. Proposition. Let $\mathbb{L}_\mathbb{R}^\vee = \text{Hom}(\mathbb{L}, \mathbb{R})$ denote the real dual of \mathbb{L} . Identify the real dual $\text{Hom}(\mathbb{Z}^N, \mathbb{R})$ of \mathbb{Z}^N with \mathbb{R}^N by means of the standard dot product.

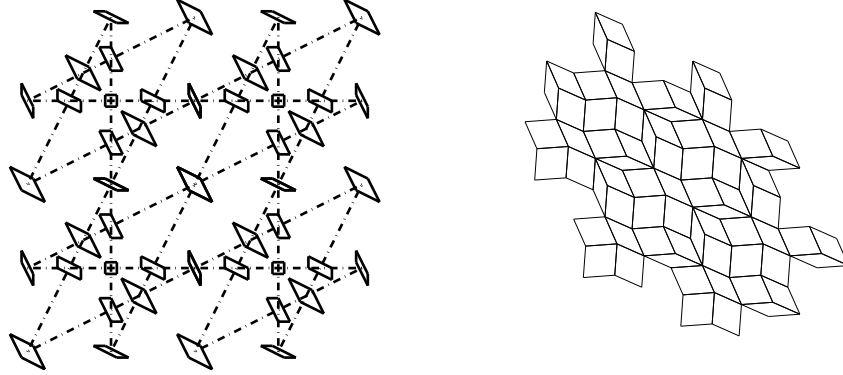


Figure 7: *converting grid to tiling for B_2 from Figure 3*

Then the linear map $\mathbb{R}^N \rightarrow \mathbb{L}_{\mathbb{R}}^{\vee}$ which is dual to the inclusion $\mathbb{L} \rightarrow \mathbb{Z}^N$, restricts to a homeomorphism $\mathcal{S} \xrightarrow{\sim} \mathbb{L}_{\mathbb{R}}^{\vee}$.

Proof. Let $\mathbf{b}_1, \dots, \mathbf{b}_N \in \mathbb{L}_{\mathbb{R}}^{\vee}$ denote the images of the standard basis vectors of \mathbb{R}^N . After identifying in the obvious way, the real plane $\mathbb{L}_{\mathbb{R}}$ with the real 2-plane $\lambda + \mathbb{L}_{\mathbb{R}}$ in \mathbb{R}^N one obtains in $\mathbb{L}_{\mathbb{R}}$ an N -grid in which the grid lines $\mathcal{L}_{i,k}^{\lambda}$ are perpendicular to \mathbf{b}_i . After choosing a basis for \mathbb{L} and taking the dual basis for $\mathbb{L}_{\mathbb{R}}^{\vee}$ we may identify $\mathbb{L}_{\mathbb{R}}$ and $\mathbb{L}_{\mathbb{R}}^{\vee}$ with \mathbb{R}^2 . The term “perpendicular” then means perpendicular with respect to the standard inner product on \mathbb{R}^2 .

Next draw for each intersection point of grid lines, say $\mathbf{x} = \mathcal{L}_{i,k}^{\lambda} \cap \mathcal{L}_{j,m}^{\lambda}$, a parallelogram with centre \mathbf{x} and sides $\epsilon \mathbf{b}_i$ and $\epsilon \mathbf{b}_j$. Here the positive real number ϵ is so small that the parallelograms obtained from all grid intersection points are disjoint; see Figure 7 for an example. It is clear from this figure how one can glue the parallelograms of two consecutive intersection points on a grid line along their sides perpendicular to the grid line. The result of this glueing is then the same as the image (scaled with a factor ϵ) of the surface \mathcal{S} under the projection $\mathbb{R}^N \rightarrow \mathbb{L}_{\mathbb{R}}^{\vee}$. ■

It is obvious from the construction that the group \mathbb{L} acts by translations on the point set \mathcal{S}^0 and on the surface \mathcal{S} , preserving the types of the squares and their sides. The cell structure on \mathcal{S} given by the squares, their sides and vertices induces therefore on \mathcal{S}/\mathbb{L} a cell structure. The following proposition counts the cells on \mathcal{S}/\mathbb{L} .

6.5. Proposition. *Let B be a $2 \times N$ -matrix such that its rows are a \mathbb{Z} -basis for \mathbb{L} . Let $\mathbf{b}_1, \dots, \mathbf{b}_N$ be the columns of this matrix. Then on \mathcal{S}/\mathbb{L}*

1. *the number of 2-cells of type (i, j) is $|\det(\mathbf{b}_i, \mathbf{b}_j)|$.*
2. *the number of 1-cells of type i is $\sum_{j=1}^N |\det(\mathbf{b}_i, \mathbf{b}_j)|$.*
3. *the number of 0-cells is $\sum_{1 \leq i < j \leq N} |\det(\mathbf{b}_i, \mathbf{b}_j)|$.*

Proof. The counts can be made on the dual structure, which is given by the intersecting grid lines on $\mathbb{L}_{\mathbb{R}}$. Let B_{ij} denote the 2×2 -matrix with columns \mathbf{b}_i and \mathbf{b}_j . Then 1. amounts to counting for $\lambda_i, \lambda_j \in \mathbb{R}$ the number of elements in the set $\{\mathbf{x} = (x_1, x_2) \in \mathbb{R}^2 \mid 0 \leq x_1, x_2 < 1, \mathbf{x} B_{ij} + (\lambda_i, \lambda_j) \in \mathbb{Z}^2\}$. Since there is a bijection between this set and the coset space $\mathbb{Z}^2 / \mathbb{Z}^2 B_{ij}$, the number of elements is $|\det B_{ij}|$. The number of 1-cells of type i is equal to the number of intersection points of the i -th grid with the other grids. In view of 1. this number is therefore as stated in 2. Knowing the numbers of 0- and 1-cells on the 2-torus $\mathbb{L}_{\mathbb{R}} / \mathbb{L}$ one computes the number of 2-cells from the fact that the Euler characteristic of a 2-torus is 0. \blacksquare

6.6. Second step. For the constructions in 6.1 and 6.3 we may randomly choose a non-resonant $\lambda \in \mathbb{R}^N$. Once we have constructed the set \mathcal{S}^0 and surface \mathcal{S} we modify it by *elementary transformations*. For such an elementary transformation we need a point $\mathbf{p}_0 \in \mathcal{S}^0$ such that there are exactly three points $\mathbf{p}_1, \mathbf{p}_2, \mathbf{p}_3$ in \mathcal{S}^0 at distance 1 from \mathbf{p}_0 and such that the three points $\mathbf{p}_1 + \mathbf{p}_2 - \mathbf{p}_0, \mathbf{p}_1 + \mathbf{p}_3 - \mathbf{p}_0$ and $\mathbf{p}_2 + \mathbf{p}_3 - \mathbf{p}_0$ also lie in \mathcal{S}^0 . These seven points are the vertices of three squares in \mathcal{S} . The elementary transformation now replaces \mathbf{p}_0 by $\mathbf{p}'_0 := \mathbf{p}_1 + \mathbf{p}_2 + \mathbf{p}_3 - 2\mathbf{p}_0$ and replaces the three squares by the three squares in \mathbb{R}^N with vertex configuration $\{\mathbf{p}_1, \mathbf{p}_2, \mathbf{p}_3, \mathbf{p}_1 + \mathbf{p}_2 - \mathbf{p}_0, \mathbf{p}_1 + \mathbf{p}_3 - \mathbf{p}_0, \mathbf{p}_2 + \mathbf{p}_3 - \mathbf{p}_0, \mathbf{p}'_0\}$; see Figure 8. In order to preserve \mathbb{L} -periodicity

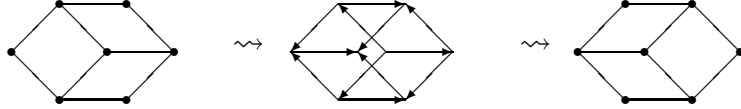


Figure 8: *An elementary transformation*

we perform this transformation simultaneously at all configurations $\{\mathbf{p}_0 + \ell, \mathbf{p}_1 + \ell, \mathbf{p}_2 + \ell, \mathbf{p}_3 + \ell\}$ with $\ell \in \mathbb{L}$.

After this elementary transformation we obtain a surface \mathcal{S}' in \mathbb{R}^N which is the union of all unit squares with vertices in the set \mathcal{S}'^0 , obtained from \mathcal{S}^0 by replacing the points $\mathbf{p}_0 + \ell$ by $\mathbf{p}_1 + \mathbf{p}_2 + \mathbf{p}_3 - 2\mathbf{p}_0 + \ell$ for all $\ell \in \mathbb{L}$.

The surface \mathcal{S}' , in turn, can be further modified by elementary transformations: just replace in the above construction \mathcal{S}^0 by \mathcal{S}'^0 and \mathbf{p}_0 by an appropriate point of \mathcal{S}'^0 .

6.7. Third step. After starting the construction in 6.3 with a randomly chosen non-resonant $\lambda \in \mathbb{R}^N$ one can create by repeated elementary transformations many surfaces \mathcal{S} each of which is the union of unit squares with vertices in an \mathbb{L} -invariant subset \mathcal{S}^0 of \mathbb{Z}^N and which is mapped homeomorphically onto $\mathbb{L}_{\mathbb{R}}^{\vee}$ by the projection $\mathbb{R}^N \rightarrow \mathbb{L}_{\mathbb{R}}^{\vee}$. Moreover the numbers of cells

on each of these surfaces are still the same as in Proposition 6.5.

The number of surfaces one can make in this way is finite and it is possible to generate (by computer) a complete list.

6.8. Remark. The list of surfaces produced in 6.7 is, up to permutation of its entries, independent of the choice of $\lambda \in \mathbb{R}^N$ at the start of the algorithm. This can be seen as follows. Fix i , $1 \leq i \leq N$. Take $\lambda \in \mathbb{R}^N$ and let $\lambda_t = \lambda + t\mathbf{e}_i$ for $t \in \mathbb{R}$. Set $t_1 = \min\{t \in \mathbb{R}_{>0} \mid \lambda_t \text{ is not non-resonant}\}$ and $t_2 = \min\{t \in \mathbb{R}_{>t_1} \mid \lambda_t \text{ is not non-resonant}\}$. Then the surface \mathcal{S}_t constructed from λ_t in 6.3 is equal to the surface \mathcal{S}_0 for $0 < t < t_1$. Figure 9 shows how the grid locally changes as t passes through t_1 . Comparing Figures 9 and 8

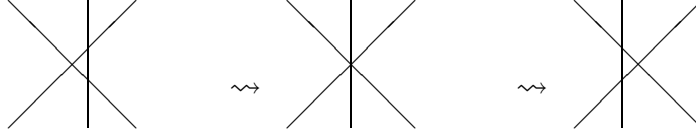


Figure 9: *Local change in grid at resonance*

one sees that such a local change of the grid corresponds to an elementary transformation of the surface \mathcal{S}_0 . Thus the surfaces \mathcal{S}_t with $t_1 < t < t_2$ are obtained from \mathcal{S}_0 by a number of elementary transformations.

Since any two non-resonant $\lambda, \lambda' \in \mathbb{R}^N$ can be moved to a common value by coordinatewise changes as above we conclude that the surfaces \mathcal{S} and \mathcal{S}' obtained in 6.3 from λ and λ' , respectively, are related by elementary transformations, and that, hence, the lists of surfaces which the algorithm produces from start values λ and λ' are the same, up to possibly a permutation of the entries.

6.9. Definition. We say that a surface \mathcal{S} on this list is *perfect* if the function $\mathbf{s} : \mathbb{R}^N \rightarrow \mathbb{R}$, $\mathbf{s}(z_1, \dots, z_N) = z_1 + \dots + z_N$, takes only three values on the set \mathcal{S}^0 of vertices in \mathcal{S} . In that case these three values are consecutive integers, say $a + 1, a, a - 1$. We denote by \mathcal{S}^\bullet (resp. \mathcal{S}^* resp. \mathcal{S}°) the set of vertices where \mathbf{s} takes the value $a + 1$ (resp. a resp. $a - 1$) and say that the vertices in \mathcal{S}^\bullet are *black*, those in \mathcal{S}° are *white* and those in \mathcal{S}^* are *grey*. Each of these sets is invariant under the translation action of \mathbb{L} .

6.10. Remark. I have at present no proof that for every rank 2 subgroup $\mathbb{L} \subset \mathbb{Z}^N$ as in 2.1 the above construction indeed yields at least one perfect surface. On the other hand, in all examples I investigated the computer produced at least one perfect surface. It would also be very interesting to know which perfect surfaces can arise already in the first step 6.3 of the construction, by choosing λ appropriately (instead of at random).

6.11. For every surface \mathcal{S} in the list of 6.7 one has the graph $\widehat{\Gamma}$ with set of vertices \mathcal{S}^0 and arrows given by the diagonals in the squares, oriented such that in a square of type (i, j) the oriented diagonals are $\mathbf{e}_i + \mathbf{e}_j$ and $\text{sign}(\det(\mathbf{b}_i, \mathbf{b}_j))(\mathbf{e}_i - \mathbf{e}_j)$. The advantage of having \mathcal{S} embedded in \mathbb{R}^N is that the vertices and the arrows in these graphs are actual points and vectors in \mathbb{R}^N . If the surface \mathcal{S} is perfect, every square in \mathcal{S} has one vertex in \mathcal{S}^\bullet , one in \mathcal{S}° and two vertices in \mathcal{S}^* . One of its diagonals goes from the white to the black vertex and the other diagonal connects the two grey vertices. The graph $\widehat{\Gamma}$ therefore is the disjoint union of two oriented graphs $\widehat{\Gamma}^{\bullet\circ}$ and $\widehat{\Gamma}^*$, with vertex sets $\mathcal{S}^\bullet \cup \mathcal{S}^\circ$ and \mathcal{S}^* , respectively. The graph $\widehat{\Gamma}^{\bullet\circ}$ is a *bi-partite graph*, i.e. its vertex set is the disjoint union of two sets (the black resp. white vertices) and with edges connecting only vertices of different colors.

There is a natural duality between $\widehat{\Gamma}^{\bullet\circ}$ and $\widehat{\Gamma}^*$: every vertex of $\widehat{\Gamma}^{\bullet\circ}$ lies in a unique connected component of $\mathcal{S} \setminus \widehat{\Gamma}^*$ and vice versa. Moreover the boundaries of these connected components are polygons and an arrow between two nodes in one graph is a common side of the corresponding polygons for the other graph.

6.12. The perfect surface \mathcal{S} is mapped homeomorphically onto $\mathbb{L}_{\mathbb{R}}^\vee$ by the projection $\mathbb{R}^N \rightarrow \mathbb{L}_{\mathbb{R}}^\vee$, which is dual to the inclusion $\mathbb{L} \hookrightarrow \mathbb{Z}^N$. This projection maps \mathbf{e}_i to \mathbf{b}_i , for $i = 1, \dots, N$. One may however pre-compose this projection with the linear map $\mathbb{R}^N \rightarrow \mathbb{R}^N$, $\mathbf{e}_i \mapsto \frac{1}{\|\mathbf{b}_i\|} \mathbf{e}_i$, $1 \leq i \leq N$. The composite linear map $\mathbb{R}^N \rightarrow \mathbb{L}_{\mathbb{R}}^\vee$ maps the tiling by squares on the surface \mathcal{S} piecewise linearly and homeomorphically onto a tiling of $\mathbb{L}_{\mathbb{R}}^\vee$ by rhombi. It maps \mathbb{L} isomorphically onto a lattice $\overline{\mathbb{L}}$ in $\mathbb{L}_{\mathbb{R}}^\vee$ and it maps the graphs $\widehat{\Gamma}^{\bullet\circ}$ and $\widehat{\Gamma}^*$ ‘isomorphically’ onto $\overline{\mathbb{L}}$ -periodic graphs $\overline{\Gamma}^{\bullet\circ}$ and $\overline{\Gamma}^*$ in the plane $\mathbb{L}_{\mathbb{R}}^\vee$. In the literature $\overline{\Gamma}^{\bullet\circ} \subset \mathbb{L}_{\mathbb{R}}^\vee$ is called a *periodic dimer model* or *periodic brane tiling*; see for instance [4, 5, 12, 13, 14, 15].

6.13. Definition. All structures in 6.11 are invariant under translation by vectors in \mathbb{L} . Passing to the orbit space we obtain from a perfect surface \mathcal{S} the 2-dimensional torus $\mathcal{T} = \mathcal{S}/\mathbb{L}$ (i.e. compact oriented surface of genus 1 without boundary). Embedded in this torus are the two graphs $\Gamma^{\bullet\circ} = \widehat{\Gamma}^{\bullet\circ}/\mathbb{L}$ and $\Gamma^* = \widehat{\Gamma}^*/\mathbb{L}$, which are dual to each other. Note that 6.12 also yields $\mathcal{T} = \mathbb{L}_{\mathbb{R}}^\vee/\overline{\mathbb{L}}$, $\Gamma^{\bullet\circ} = \overline{\Gamma}^{\bullet\circ}/\overline{\mathbb{L}}$ and $\Gamma^* = \overline{\Gamma}^*/\overline{\mathbb{L}}$.

After Grothendieck one calls $(\mathcal{T}, \Gamma^*, \Gamma^{\bullet\circ})$ a *dessin d’enfants* [18, 22].

6.14. Example. Figure 10 shows two drawings of the dessin $(\mathcal{T}, \Gamma^*, \Gamma^{\bullet\circ})$ for B_{10} from Figure 3; or, rather, it shows a lifting of this dessin to the plane $\mathbb{L}_{\mathbb{R}}^\vee$ with basis so that the period lattice $\overline{\mathbb{L}}$ becomes just \mathbb{Z}^2 . It also shows Γ^* as

an unembedded quiver. *Note however that this is not the same as the quiver Q in case B_{10} in Figure 3.*

The quiver in Figure 10 is in fact the quiver for the singularity $\mathbb{C}^3/\mathbb{Z}_6$ where a generator of the cyclic group \mathbb{Z}_6 acts on \mathbb{C}^3 as multiplication by the diagonal matrix $\text{diag}(e^{2\pi i/6}, e^{2\pi i/3}, e^{2\pi i/2})$. Also the brane tiling picture in Figure 10 appears in [13] §3 in connection with the singularity $\mathbb{C}^3/\mathbb{Z}_6$.

This difference between [13] and our approach comes, because we still have to perform the untwist, as is explained below.

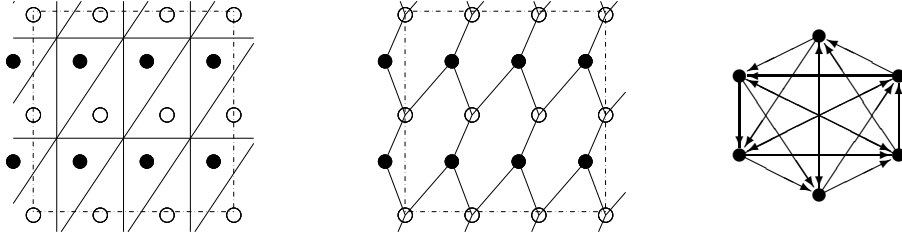


Figure 10: *Two versions of the dessin $(\mathcal{T}, \Gamma^*, \Gamma^{\bullet\circ})$ for B_{10} from Figure 3. The dashed square is the period parallelogram. The picture on the left shows how the quiver on the right is embedded in a 2-torus.*

6.15. The quiver Γ^* in 6.13 is not the Plücker quiver of \mathbb{L} , defined in 2.5. The latter appears in the current setting through the *zigzag loops*, as follows. Let \mathcal{S} be a perfect surface. Fix $i \in \{1, \dots, N\}$. In every square on \mathcal{S} which has two sides parallel to \mathbf{e}_i draw the line segment connecting the midpoints of these two sides. If the square has type (i, j) this line segment is oriented so that it is a translate of the vector $\text{sign}(\det(\mathbf{b}_i, \mathbf{b}_j))\mathbf{e}_j$. The union of these line segments projects to an oriented closed curve on \mathcal{T} , called the *i -th zigzag loop*. Note that this zigzag loop may consist of several connected components.

According to Proposition 6.5 the i -th and j -th zigzag loops on \mathcal{T} intersect in exactly $|\det(\mathbf{b}_i, \mathbf{b}_j)|$ points. *Thus we see that the nodes of the Plücker quiver can be identified with the zigzag loops on \mathcal{T} and the arrows between two nodes are the intersection points of the corresponding zigzag loops.* The orientation of the arrows follows from the orientation of the zigzag loops and can in pictures be indicated as an over/undercrossing of the zigzag loops.

Figure 11 shows the zigzag loops for the dessin in Figure 10.

6.16. Final untwist. Pictures like Figure 11 can be viewed as showing an oriented surface with boundary, in which the connected components of the zigzag loops are the connected components of the boundary and which is embedded in three space in a twisted way so that the black dots are on

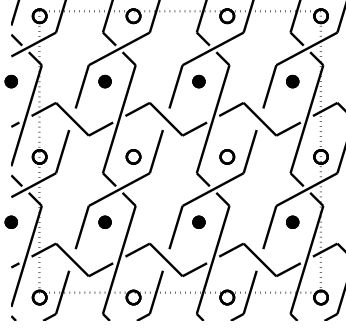


Figure 11: *The zigzag loops for the dessin in Figure 10*

one side of the surface and the white dots are on the other side. This surface comes with a tiling by helices as shown in Figure 12.

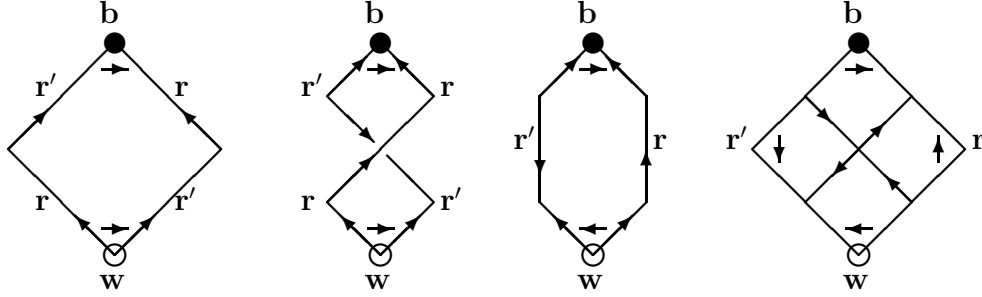


Figure 12: Untwisting: *from left to right: original square tile, helix tile, untwisted helix tile, untwisted helix completed to square tile.*

One can ‘untwist’ the helix tiles and complete the untwisted helix tiles to squares as indicated in Figure 12. The effect is that the boundary cycles are being capped off by discs. The result is an oriented surface \mathcal{M} without boundary which is tiled by squares with one black, one white and two red vertices. The black-white diagonals give an embedding of the bipartite graph $\Gamma^{\bullet\circ}$ into \mathcal{M} . The red-red diagonals give an embedding of the quiver \mathbf{Q} into \mathcal{M} (if all zigzag loops have just one connected component; otherwise some points on the surface must be pinched together).

The untwisting procedure is described in [4] §5 via examples, pictures and visual inspection. Here we want to build the ‘untwisted surface’ by simply reinterpreting the combinatorial data of the tiling of the torus \mathcal{T} , i.e. the \mathbb{L} -periodic tiling of the perfect surface \mathcal{S} by unit squares taken modulo \mathbb{L} (see 6.9, 6.13). Let \mathbf{B} (resp. \mathbf{W}) denote the set of black (resp. white) vertices. There is a bijection between the set of tiles and the set E of arrows of the quiver \mathbf{Q} and we can refer to tiles as $e \in E$. A tile e has one black vertex $\mathbf{b}(e)$ and one white vertex $\mathbf{w}(e)$. A tile e is the image of a unit square with sides parallel to two of the basis vectors $\mathbf{e}_1, \dots, \mathbf{e}_N$; let us denote the indices of this (unordered) pair of basis vectors as a 2-element subset $\{\mathbf{r}(e), \mathbf{r}'(e)\}$ of

$\{1, \dots, N\}$. Thus the tiling on \mathcal{T} yields the list of quadruples

$$\mathbb{M} = \{ (\mathbf{b}(e), \mathbf{w}(e), \mathbf{r}(e), \mathbf{r}'(e)) \}_{e \in E}. \quad (26)$$

Now, for every $e \in E$ we take a unit square \square_e and attach labels $\mathbf{b}(e)$, $\mathbf{w}(e)$, $\mathbf{r}(e)$, $\mathbf{r}'(e)$ and colors black, white, red, red, respectively, to its vertices such that the vertices labeled $\mathbf{b}(e)$ and $\mathbf{w}(e)$ are not adjacent. If two such squares \square_e and $\square_{e'}$ have equal labels on two adjacent vertices, we glue \square_e and $\square_{e'}$ along the corresponding sides. The result of this glueing is a surface $\widetilde{\mathcal{M}}$ tiled with squares.

On the surface $\widetilde{\mathcal{M}}$ there is for every $\mathbf{b} \in \mathbf{B}$ one black point with label \mathbf{b} and for every $\mathbf{w} \in \mathbf{W}$ there is one white point with label \mathbf{w} . However for $i \in \{1, \dots, N\}$ there may be several red points with label i . We finally obtain the desired surface \mathcal{M} by identifying for every $i \in \{1, \dots, N\}$ the red points with label i .

6.17. Proposition. *The surface $\widetilde{\mathcal{M}}$, and hence also \mathcal{M} , is oriented.*

Proof. Cut the square \square_e in four pieces like in the right-hand picture of Figure 12. Then for fixed $\mathbf{b} \in \mathbf{B}$ the small squares with black vertex \mathbf{b} are glued together to a polygon isomorphic to the polygon in \mathcal{T} formed by the unit squares with one vertex \mathbf{b} . Similarly, for fixed $\mathbf{w} \in \mathbf{W}$ the small squares with white vertex \mathbf{w} are glued together to a polygon isomorphic to the polygon in \mathcal{T} formed by the unit squares with one vertex \mathbf{w} but with the orientation reversed. For $i \in \{1, \dots, N\}$ the small squares with red vertex i are glued together to a number of disjoint polygons, one for every connected component of the i -th zigzag loop and with oriented boundary ‘equal to’ that component. It is now clear from Figure 12 that these polygons are oriented consistently so that $\widetilde{\mathcal{M}}$ is oriented. ■

6.18. Conclusion. *The surface \mathcal{M} is tiled with squares so that the black-white diagonals form a bi-partite graph isomorphic to the bi-partite graph $\Gamma^{\bullet\circ}$ in 6.13, while the red-red diagonals form a graph isomorphic to the quiver \mathbf{Q} .*

6.19. Example. The list \mathbb{M} (26) which our algorithm produces for model IV of dP_3 , i.e. example B_{10} from Figure 3, is

e	:	1	2	3	4	5	6	7	8	9	10	11	12	13	14	15	16	17	18
$\mathbf{b}(e)$:	6	5	1	2	4	3	1	5	3	6	4	2	5	6	1	2	3	4
$\mathbf{w}(e)$:	5	6	2	1	3	4	3	1	5	2	6	4	5	6	1	2	3	4
$\mathbf{r}(e)$:	2	2	3	3	4	4	1	1	1	1	1	1	5	6	5	6	5	6
$\mathbf{r}'(e)$:	1	1	1	1	1	1	5	5	5	6	6	6	2	2	3	3	4	4

The surface \mathcal{M} with the corresponding tiling by kites (instead of squares) is shown in the left-hand picture in Figure 13. The right-hand picture in Figure

13 shows the bi-partite graph $\Gamma^{\bullet\circ}$ and the quiver Q embedded in \mathcal{M} . Note that this quiver is indeed the same as the one for example B_{10} in Figure 13.

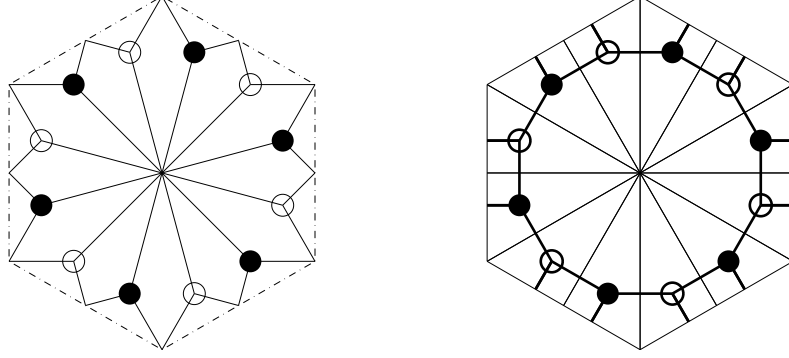


Figure 13: Surface \mathcal{M} with kite tiling (left) and quiver Q and bipartite graph $\Gamma^{\bullet\circ}$ (right) for case B_{10} in Figure 4 (= model IV of dP_3). The surface \mathcal{M} is obtained by identifying opposite sides of the hexagon.

7 Perfect matchings and the secondary fan.

7.1. Definition. (see e.g. [17, 16, 20]) A *perfect matching* P on a bi-partite graph $\Gamma^{\bullet\circ}$ (also known as a *dimer configuration*) is a subset of the edges of $\Gamma^{\bullet\circ}$ such that every node of $\Gamma^{\bullet\circ}$ is incident to exactly one edge in P .

7.2. Theorem. Consider a subgroup $\mathbb{L} \subset \mathbb{Z}^N$ as in 2.1. Let $\Gamma^{\bullet\circ}$ be a bi-partite graph which is obtained from $\mathbb{L} \subset \mathbb{Z}^N$ as explained in Section 6, and in Definition 6.13 in particular. Let C be a 2-dimensional cone in the secondary fan of $\mathbb{L} \subset \mathbb{Z}^N$ and let L_C be the corresponding collection of 2-element subsets of $\{1, \dots, N\}$ as in 3.2 and 3.3. Identify E with the set of edges of $\Gamma^{\bullet\circ}$. Then, with the notation as in (26), the set

$$P_C = \{e \in E \mid \{\mathbf{r}(e), \mathbf{r}'(e)\} \in L_C\} \quad (27)$$

is a perfect matching on $\Gamma^{\bullet\circ}$.

Proof. Consider a perfect surface $\mathcal{S} \subset \mathbb{R}^N$ as in 6.9. The map $\pi : \mathbb{R}^N \rightarrow \mathbb{L}_{\mathbb{R}}^{\vee}$ which is dual to the inclusion $\mathbb{L} \hookrightarrow \mathbb{Z}^N$ projects \mathcal{S} homeomorphically onto the plane $\mathbb{L}_{\mathbb{R}}^{\vee}$. The tiling of \mathcal{S} by unit squares gives a tiling of $\mathbb{L}_{\mathbb{R}}^{\vee}$ by parallelograms. A unit square with edges \mathbf{e}_i and \mathbf{e}_j projects onto a parallelogram with edges \mathbf{b}_i and \mathbf{b}_j . Now let C be a 2-dimensional cone of the secondary fan (see 3.2) and let \mathbf{w} be a white vertex of the tiling. By translating the origin of the secondary fan to \mathbf{w} one sees that there is exactly one parallelogram

with vertex \mathbf{w} and with edges \mathbf{b}_i and \mathbf{b}_j such that $C \subset \mathbb{R}_{\geq 0}\mathbf{b}_i + \mathbb{R}_{\geq 0}\mathbf{b}_j$, i.e. such that $\{i, j\} \in L_C$. This shows that there is exactly one element of P_C incident to \mathbf{w} , namely the black-white diagonal of this parallelogram. A similar argument works for the black vertices. ■

7.3. Corollary. *In the situation of Theorem 7.2 the number of black vertices and the number of white vertices are both equal to the number $\text{vol}_{\mathcal{A}}$ in (19).*

Proof. The number of black (resp. white) vertices of $\Gamma^{\bullet\circ}$ is equal to the number of edges in any perfect matching. This holds in particular for the perfect matching P_C corresponding to a 2-dimensional cone C in the secondary fan. The result now follows from (27), (4) and (19). ■

The following result was also derived in [4] §5.1.

7.4. Corollary. *The genus of the surface \mathcal{M} in 6.16 is equal to the number of lattice points in the interior of the secondary polytope Δ in (8).*

Proof. The number of 1-cells in the tiling of \mathcal{M} is twice the number of 2-cells. According to Proposition 6.5 the number of 2-cells is $\sum_{1 \leq i < j \leq N} |\det(\mathbf{b}_i, \mathbf{b}_j)|$. The number of 0-cells is, according to Corollary 7.3 and Formula (19) equal to $N + 2 \sum_{\{i,j\} \in L_C} |\det(\mathbf{b}_i, \mathbf{b}_j)|$. The desired result now follows from Corollary 3.10 and a calculation of the Euler characteristic $2 - 2 \text{genus}(\mathcal{M})$. ■

8 Kasteleyn matrix, bi-adjacency matrix, 3-constellation and superpotential.

8.1. In 6.12 we found the $\overline{\mathbb{L}}$ -periodic bi-partite graph $\overline{\Gamma}^{\bullet\circ}$ in the plane $\mathbb{L}_{\mathbb{R}}^{\vee}$. Periodic bi-partite graphs in the plane are also known as *periodic dimer models*. One of the main tools for studying periodic dimer models is the *Kasteleyn matrix*. It is usually defined as an adjacency matrix with extra factors x, x^{-1}, y, y^{-1} for edges crossing the sides of a fundamental parallelogram and determined by visual inspection of a picture of the periodic dimer model; see e.g. [17, 13, 15]. The purpose of the extra factors is to keep track of the homology class of a closed path on the bi-partite graph $\Gamma^{\bullet\circ}$ in the torus \mathcal{T} (see 6.13). We obtained $\overline{\Gamma}^{\bullet\circ} \subset \mathbb{L}_{\mathbb{R}}^{\vee}$ as the projection of the black-white diagonals in the tiling of the perfect surface \mathcal{S} by unit squares. The advantage of having \mathcal{S} embedded in \mathbb{R}^N is that these diagonals are actual vectors in \mathbb{Z}^N and that points lying on paths formed by these diagonals are simply given by vector addition. Thus all edges become “equally responsible” for the periodicity. An edge which is the diagonal in a square of type (i, j) contributes $\mathbf{e}_i + \mathbf{e}_j$.

Thus we are led to a reformulation of the Kasteleyn matrix of the dimer model $(\mathcal{T}, \Gamma^{\bullet\circ})$ in terms of the combinatorial data given as the list \mathbb{M} in

Equation (26). As this same list is used in 6.16 for building the surface \mathcal{M} we call the same matrix also the bi-adjacency matrix of the dessin $(\mathcal{M}, \mathbf{Q})$.

8.2. Definition. From the list $\mathbb{M} = \{ (\mathbf{b}(e), \mathbf{w}(e), \mathbf{r}(e), \mathbf{r}'(e)) \}_{e \in E}$ in (26) and a function $\varpi : E \rightarrow \mathbb{C}$ on the set of edges of the quiver \mathbf{Q} we construct a matrix \mathbb{K}^ϖ with rows indexed by the set of black vertices \mathbf{B} , columns indexed by the set of white vertices \mathbf{W} and with entries in the polynomial ring $\mathbb{C}[u_1, \dots, u_N]$:

$$(\mathbf{b}, \mathbf{w})\text{-entry of } \mathbb{K}^\varpi = \sum_{e \in E: \mathbf{b}(e)=\mathbf{b}, \mathbf{w}(e)=\mathbf{w}} \varpi(e) u_{\mathbf{r}(e)} u_{\mathbf{r}'(e)}. \quad (28)$$

We use for \mathbb{K}^ϖ the name *Kasteleyn matrix of the dimer model* $(\mathcal{T}, \Gamma^\bullet)$ as well as the name *bi-adjacency matrix of the dessin* $(\mathcal{M}, \mathbf{Q})$.

8.3. Example. Although the relation between the list \mathbb{M} and the matrix \mathbb{K}^ϖ is so straightforward, that there seems no point in writing here the matrix \mathbb{K}^ϖ for Example 6.19, we do present this \mathbb{K}^ϖ here to compare it with results in the literature.

bi-adjacency matrix \mathbb{K}^ϖ for model IV of $dP_3 =$

$$\begin{bmatrix} \varpi_{15} u_3 u_5 & \varpi_3 u_1 u_3 & \varpi_7 u_1 u_5 & 0 & 0 & 0 \\ \varpi_4 u_1 u_3 & \varpi_{16} u_3 u_6 & 0 & \varpi_{12} u_1 u_6 & 0 & 0 \\ 0 & 0 & \varpi_{17} u_4 u_5 & \varpi_6 u_1 u_4 & \varpi_9 u_1 u_5 & 0 \\ 0 & 0 & \varpi_5 u_1 u_4 & \varpi_{18} u_4 u_6 & 0 & \varpi_{11} u_1 u_6 \\ \varpi_8 u_1 u_5 & 0 & 0 & 0 & \varpi_{13} u_2 u_5 & \varpi_2 u_1 u_2 \\ 0 & \varpi_{10} u_1 u_6 & 0 & 0 & \varpi_1 u_1 u_2 & \varpi_{14} u_2 u_6 \end{bmatrix}$$

(with ϖ_e denoting $\varpi(e)$). In view of the discussion in Example 6.14 this bi-adjacency matrix for model IV of dP_3 should be somehow the same as the Kasteleyn matrix for the singularity $\mathbb{C}^3/\mathbb{Z}_6$ in [13] Equation (3.5):

$$K(z, w) = \begin{bmatrix} w & -1 & 0 & -w & 0 & 0 \\ 0 & 1 & -1 & 0 & -1 & 0 \\ -1 & 0 & 1 & 0 & 0 & -1 \\ -zw & 0 & 0 & w & -1 & 0 \\ 0 & -z & 0 & 0 & 1 & -1 \\ 0 & 0 & -z & -1 & 0 & 1 \end{bmatrix}.$$

Indeed, by dividing the first, third and fifth column of \mathbb{K}^ϖ by u_5 and subsequently setting $u_5 = z^{-1}$, $u_3 = w$, $u_1 = u_2 = u_4 = u_6 = 1$, and appropriately setting $\varpi_e = \pm 1$ one obtains a matrix which up to a permutation of rows and columns is $K(z, w)$. This way of getting $K(z, w)$ from \mathbb{K}^ϖ is nothing but passing from homogeneous to inhomogeneous coordinates.

8.4. Definition.(cf. [18] Definition 1.1.1.) A *3-constellation* (E, σ_0, σ_1) consists of a finite set E and two permutations σ_0, σ_1 of E such that the permutation group generated by σ_0, σ_1 acts transitively on E .

8.5. Notations. The cycle notation $(i_1 \ i_2 \dots i_{k-1} \ i_k)$ denotes the permutation ρ such that $\rho(i_j) = i_{j+1}$ for $j = 1, \dots, k-1$ and $\rho(i_k) = i_1$. By a *cycle* of a permutation σ we mean an orbit of the group generated by σ . We denote the set of cycles of σ by E_σ . In the product $\sigma\tau$ of two permutations σ and τ one first applies τ ; so $(\sigma\tau)(i) = \sigma(\tau(i))$.

8.6. Definition. For our purposes we do not need the most general notion of a superpotential for a quiver. The superpotentials we need are just notational reformulations of 3-constellations. The *superpotential attached to a 3-constellation* (E, σ_0, σ_1) is the following polynomial W in non-commuting variables X_e ($e \in E$):

$$W = \sum_{\gamma \in E_{\sigma_0}} \mathbf{X}_\gamma - \sum_{\gamma \in E_{\sigma_1}} \mathbf{X}_\gamma,$$

where $\mathbf{X}_\gamma := X_{i_1} X_{i_2} \dots X_{i_k}$ for a cyclic permutation $\gamma = (i_1 \ i_2 \dots i_k)$.

8.7. Definition. The *3-constellation* (E, σ_0, σ_1) associated with the dessin $(\mathcal{M}, \mathbf{Q})$ in 6.18 is the following. E is the set of arrows of the quiver \mathbf{Q} . Every $e \in E$ is a path p_e on \mathcal{M} . Every connected component of $\mathcal{M} \setminus \cup_{e \in E} p_e$ has an oriented boundary which can be viewed as a cyclic permutation of elements of E . Then σ_0 (resp. σ_1) is the composition of the cyclic permutations which are boundaries of connected components containing a black (resp. white) point.

8.8. Remark. In the same way one associates a 3-constellation with the dessin (\mathcal{T}, Γ^*) in 6.13. It is obvious from the untwisting procedure in 6.16 that, if (E, σ_0, σ_1) is the 3-constellation associated with the dessin $(\mathcal{M}, \mathbf{Q})$, then $(E, \sigma_0, \sigma_1^{-1})$ is the 3-constellation associated with the dessin (\mathcal{T}, Γ^*) .

8.9. It is obvious that the 3-constellation (E, σ_0, σ_1) associated with the dessin $(\mathcal{M}, \mathbf{Q})$ contains the complete instructions for building \mathcal{M} : for every cycle of σ_0 and every cycle of σ_1 take a (convex planar) polygon with sides labeled by the elements in the cycle in their cyclic order. Next glue these polygons by identifying sides with the same label. The sides of these polygons correspond to arrows of the quiver \mathbf{Q} and the vertices of these polygons correspond to vertices of \mathbf{Q} . After the above procedure of glueing polygons along their sides one must still identify points which correspond to the same vertex of \mathbf{Q} . The result is then \mathcal{M} with \mathbf{Q} embedded in it.

8.10. The 3-constellation (E, σ_0, σ_1) in 8.9 and the list \mathbb{M} in 6.16 both are completely determined by and do completely determine the dessin $(\mathcal{M}, \mathcal{Q})$. One can, however, also describe the relation between (E, σ_0, σ_1) and \mathbb{M} in a direct algebraic/combinatorial way.

For the construction of (E, σ_0, σ_1) from \mathbb{M} one first forms for $\mathbf{b} \in \mathbf{B}$, $\mathbf{w} \in \mathbf{W}$ and $i \in \{1, \dots, N\}$ the sets

$$\begin{aligned} |\sigma_{\mathbf{b}}| &= \{e \in E \mid \mathbf{b}(e) = \mathbf{b}\}, & |\sigma_{\mathbf{w}}| &= \{e \in E \mid \mathbf{w}(e) = \mathbf{w}\}, \\ |\mathbf{z}_i| &= \{e \in E \mid i \in \{\mathbf{r}(e), \mathbf{r}'(e)\}\}. \end{aligned}$$

These sets have an unoriented cyclic structure: $e, e' \in |\sigma_{\mathbf{b}}|$ (resp. $e, e' \in |\sigma_{\mathbf{w}}|$) are neighbors if and only if $\{\mathbf{r}(e), \mathbf{r}'(e)\} \cap \{\mathbf{r}(e'), \mathbf{r}'(e')\} \neq \emptyset$, while $e, e' \in |\mathbf{z}_i|$ are neighbors if and only if $\{\mathbf{b}(e), \mathbf{w}(e)\} \cap \{\mathbf{b}(e'), \mathbf{w}(e')\} \neq \emptyset$. In order to put a consistent orientation on these cyclic sets we choose one of the two possible orientations of $|\mathbf{z}_1|$. For every $\mathbf{b} \in \mathbf{B}$ we have $\sharp(|\mathbf{z}_1| \cap |\sigma_{\mathbf{b}}|) = 0$ or 2 . In the latter case $|\mathbf{z}_1| \cap |\sigma_{\mathbf{b}}|$ consists of two elements, say e and e' , which are neighbors both in $|\mathbf{z}_1|$ and in $|\sigma_{\mathbf{b}}|$. The orientation on $|\mathbf{z}_1|$ then induces an orientation on $|\sigma_{\mathbf{b}}|$ such that e is the successor of e' in $|\sigma_{\mathbf{b}}|$ if e is the successor of e' in $|\mathbf{z}_1|$. In this way the orientation on $|\mathbf{z}_1|$ induces an orientation on every $|\sigma_{\mathbf{b}}|$ and every $|\sigma_{\mathbf{w}}|$ which has a non-empty intersection with $|\mathbf{z}_1|$. Next this induces an orientation on every $|\mathbf{z}_i|$ which has a non-empty intersection with any of the already oriented sets $|\sigma_{\mathbf{b}}|$ or $|\sigma_{\mathbf{w}}|$. And so on. It is because of the geometric background of \mathbb{M} (i.e. the orientations shown in the right-hand picture in Figure 12) that we can indeed go on. In the end all sets $|\sigma_{\mathbf{b}}|$ and $|\sigma_{\mathbf{w}}|$ have an oriented cyclic structure and can be identified with cyclic permutations $\sigma_{\mathbf{b}}$ and $\sigma_{\mathbf{w}}$. The construction of the 3-constellation (E, σ_0, σ_1) is finished by setting

$$\sigma_0 = \prod_{\mathbf{b} \in \mathbf{B}} \sigma_{\mathbf{b}}, \quad \sigma_1 = \prod_{\mathbf{w} \in \mathbf{W}} \sigma_{\mathbf{w}}^{-1};$$

the reason for inverting the white cycles is shown in Figure 14

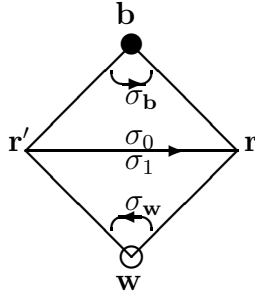


Figure 14: *orientation of cycles in 3-constellation and orientation of \mathcal{M} .*

To go from (E, σ_0, σ_1) to \mathbb{M} one views the cycles of the permutations σ_0 , σ_1 and $\sigma_0 \sigma_1^{-1}$ as elements of the sets E_{σ_0} , E_{σ_1} , $E_{\sigma_0 \sigma_1^{-1}}$, respectively, and then

sets $\mathbb{M} = \{(\mathbf{b}(e), \mathbf{w}(e), \mathbf{r}(e), \mathbf{r}'(e))\}_{e \in E}$ with

$$\begin{aligned} \mathbf{b}(e) &= \text{the cycle of } \sigma_0 \text{ which contains } e, \\ \mathbf{w}(e) &= \text{the cycle of } \sigma_1 \text{ which contains } e, \\ \mathbf{r}(e) &= \text{the cycle of } \sigma_0 \sigma_1^{-1} \text{ which contains } e, \\ \mathbf{r}'(e) &= \mathbf{r}(\sigma_1(e)). \end{aligned}$$

8.11. Example. The procedure of 8.10 converts the list \mathbb{M} in 6.19 into the 3-constellation (E, σ_0, σ_1) with

$$\begin{aligned} E &= \{1, 2, 3, 4, 5, 6, 7, 8, 9, 10, 11, 12, 13, 14, 15, 16, 17, 18\}, \\ \sigma_0 &= (3, 7, 15)(4, 12, 16)(6, 9, 17)(5, 11, 18)(2, 8, 13)(1, 10, 14), \\ \sigma_1 &= (4, 8, 15)(3, 10, 16)(5, 7, 17)(6, 12, 18)(1, 9, 13)(2, 11, 14). \end{aligned}$$

Since in this example the cycle $\mathbf{z}_1 = (1, 10, 3, 7, 5, 11, 2, 8, 4, 12, 6, 9)$ meets each of the above 3-cycles the conversion went especially fast.

The corresponding superpotential W is

$$\begin{aligned} &X_3 X_7 X_{15} + X_4 X_{12} X_{16} + X_6 X_9 X_{17} + X_5 X_{11} X_{18} + X_2 X_8 X_{13} + X_1 X_{10} X_{14} \\ &- X_4 X_8 X_{15} - X_3 X_{10} X_{16} - X_5 X_7 X_{17} - X_6 X_{12} X_{18} - X_1 X_9 X_{13} - X_2 X_{11} X_{14}. \end{aligned}$$

9 The determinant of the bi-adjacency matrix and the secondary polygon

9.1. Corollary 7.3 implies that the bi-adjacency matrix $\mathbb{K}^\varpi = (\kappa_{ij})$ of the dessin $(\mathcal{M}, \mathcal{Q})$ is a square matrix. Its determinant is by definition

$$\det \mathbb{K}^\varpi = \sum_{\tau} \text{sign}(\tau) \kappa_{i_{\tau(i)}}$$

where τ runs over the set of all bijections $\mathbf{B} \xrightarrow{\cong} \mathbf{W}$ and $\text{sign}(\tau)$ is defined as the sign of the permutation $\tau_0^{-1} \tau$ of \mathbf{B} for some reference bijection $\tau_0 : \mathbf{B} \xrightarrow{\cong} \mathbf{W}$. Of course, if we want to actually write \mathbb{K}^ϖ as a matrix, we must choose bijections between \mathbf{B} , \mathbf{W} and the set of numbers $\{1, \dots, \text{vol}_{\mathcal{A}}\}$ and that fixes τ_0 . Changing the reference bijection multiplies $\det \mathbb{K}^\varpi$ by ± 1 , but that is for our purpose unimportant. Next note that the (\mathbf{b}, \mathbf{w}) -entry of \mathbb{K}^ϖ is non-zero if and only if there is an edge of $\Gamma^{\bullet\circ}$ connecting the nodes \mathbf{b} and \mathbf{w} . So the only bijections τ that contribute to the determinant of \mathbb{K}^ϖ are the *perfect*

matchings; see Definition 7.1. Thus we find

$$\begin{aligned} \det \mathbb{K}^\varpi &= \pm \sum_{\text{perfect matchings } P} \text{sign}(P) \prod_{e \in P} w(e) u_{\mathbf{r}(e)} u_{\mathbf{r}'(e)} \\ &= \pm \sum_{\text{perfect matchings } P} \text{sign}(P) \left(\prod_{e \in P} \varpi(e) \right) \mathbf{u}^{\hat{P}} \end{aligned} \quad (29)$$

where

$$\hat{P} = \sum_{e \in P} (\mathbf{e}_{\mathbf{r}(e)} + \mathbf{e}_{\mathbf{r}'(e)}) \in \mathbb{Z}^N, \quad (30)$$

and $\mathbf{u}^{\mathbf{p}} = u_1^{p_1} \cdots u_N^{p_N}$ for $\mathbf{p} = (p_1, \dots, p_N) \in \mathbb{Z}^N$.

9.2. Definition. The *Newton polytope* of a Laurent polynomial

$$f = \sum_{(k_1, \dots, k_N) \in \mathbb{Z}^N} c_{(k_1, \dots, k_N)} u_1^{k_1} \cdots u_N^{k_N} \in \mathbb{C}[u_1^\pm, \dots, u_N^\pm]$$

is the polytope

$$\text{Newton}(f) := \text{convex hull} \left(\{(k_1, \dots, k_N) \mid c_{(k_1, \dots, k_N)} \neq 0\} \right).$$

9.3. Theorem. *The Newton polytope of the determinant of the bi-adjacency matrix \mathbb{K}^ϖ of the dessin $(\mathcal{M}, \mathbf{Q})$ is the same as the secondary polygon of $\mathbb{L} \subset \mathbb{Z}^N$ (see 3.3):*

$$\text{Newton}(\det \mathbb{K}_\varpi) = \Sigma(\mathbb{L}). \quad (31)$$

The vertices of $\text{Newton}(\det \mathbb{K}_\varpi)$ are the points \widehat{P}_C (see (30)) given by the perfect matchings P_C with C a 2-dimensional cone in the secondary fan.

Proof. If P and P' are two perfect matchings then the edges in P oriented black-to-white together with the edges in P' oriented white-to-black form a collection of closed loops on the torus \mathcal{T} in 6.13. The first homology group of this torus is \mathbb{L} . Therefore $\widehat{P} - \widehat{P}'$ lies in $\mathbb{L} \subset \mathbb{Z}^N$. This shows that $\text{Newton}(\det \mathbb{K}^\varpi)$ lies in a 2-dimensional plane in \mathbb{R}^N parallel to $\mathbb{L}_{\mathbb{R}}$.

From Equation (30) one sees that for every perfect matching P

$$\widehat{P} = \sum_{i=1}^N \# \{e \in P \mid i \in \{\mathbf{r}(e), \mathbf{r}'(e)\}\} \mathbf{e}_i,$$

i.e. the i -th coordinate of the vector \widehat{P} equals the number of edges in the perfect matching P which intersect the i -th zigzag loop (cf. 6.15). It follows from Proposition 6.5 that the number of edges of the i -th zigzag loop is

$\sum_{j=1}^N |\det(\mathbf{b}_i, \mathbf{b}_j)|$. Since consecutive edges in a zigzag loop can never intersect the same perfect matching we see that for every perfect matching P and every i

$$\#\{e \in P \mid i \in \{\mathbf{r}(e), \mathbf{r}'(e)\}\} \leq \frac{1}{2} \sum_{j=1}^N |\det(\mathbf{b}_i, \mathbf{b}_j)|. \quad (32)$$

Fix i and let C and C' be the two 2-dimensional cones in the secondary fan containing the half-line $\mathbb{R}_{\geq 0}\mathbf{b}_i$. Then $\{i, j\} \in L_C \Leftrightarrow \det(\mathbf{b}_i, \mathbf{b}_j) \geq 0$ and $\{i, j\} \in L_{C'} \Leftrightarrow \det(\mathbf{b}_i, \mathbf{b}_j) \leq 0$. Since $\sum_{j=1}^N \det(\mathbf{b}_i, \mathbf{b}_j) = 0$ we find

$$\sum_{j, \{i, j\} \in L_C} |\det(\mathbf{b}_i, \mathbf{b}_j)| = \sum_{j, \{i, j\} \in L_{C'}} |\det(\mathbf{b}_i, \mathbf{b}_j)| = \frac{1}{2} \sum_{j=1}^N |\det(\mathbf{b}_i, \mathbf{b}_j)|.$$

Thus we see that for i and the perfect matchings P_C and $P_{C'}$ Equation (32) is in fact an equality.

Fix a 2-dimensional cone C in the secondary fan. It is bounded by two half-lines $\mathbb{R}_{\geq 0}\mathbf{b}_i$ and $\mathbb{R}_{\geq 0}\mathbf{b}_{i'}$. The above argument now shows that Equation (32) is in fact an equality for the perfect matching P_C and i and for P_C and i' in place of i . Thus the point \widehat{P}_C is a vertex of $\text{Newton}(\det \mathbb{K}_w)$. This together with (32) proves:

$$\text{Newton}(\det \mathbb{K}_w) = \text{convex hull} \left(\left\{ \widehat{P}_C \mid C \text{ 2-dim. cone of secondary fan of } \mathbb{L} \right\} \right).$$

To complete the proof of (31) we note that Equations (4), (5), (27) and (30) together with Proposition 6.5 show $\widehat{P}_C = \psi_C$. \blacksquare

9.4. Example. According to [5] §8 the quiver for model II of dP_3 (i.e. case B_8 in Figure 4) affords two different superpotentials. This is confirmed by our algorithm, which yields the following two bi-adjacency matrices

$$\mathbb{K}_1^w = \begin{bmatrix} \varpi_2 u_1 u_2 & \varpi_8 u_2 u_4 & 0 & \varpi_4 u_1 u_4 \\ \varpi_{14} u_5 u_6 & \varpi_{10} u_2 u_6 & \varpi_9 u_2 u_5 & 0 \\ \varpi_6 u_1 u_6 + \varpi_7 u_2 u_3 & \varpi_{13} u_4 u_6 & \varpi_1 u_1 u_2 & \varpi_{11} u_3 u_4 \\ \varpi_{12} u_3 u_5 & 0 & \varpi_5 u_1 u_5 & \varpi_3 u_1 u_3 \end{bmatrix}$$

$$\mathbb{K}_2^w = \begin{bmatrix} \varpi_2 u_1 u_2 & \varpi_9 u_2 u_5 & 0 & \varpi_5 u_1 u_5 \\ \varpi_4 u_1 u_4 & \varpi_1 u_1 u_2 & \varpi_8 u_2 u_4 & 0 \\ \varpi_7 u_2 u_3 & \varpi_{14} u_5 u_6 & \varpi_{10} u_2 u_6 & \varpi_{12} u_3 u_5 \\ \varpi_{11} u_3 u_4 & \varpi_6 u_1 u_6 & \varpi_{13} u_4 u_6 & \varpi_3 u_1 u_3 \end{bmatrix}$$

The corresponding superpotentials are:

$$\begin{aligned} W_1 = & X_2 X_8 X_4 + X_9 X_{14} X_{10} + X_1 X_7 X_{11} X_{13} X_6 + X_3 X_{12} X_5 \\ & - X_2 X_7 X_{12} X_{14} X_6 - X_8 X_{13} X_{10} - X_1 X_9 X_5 - X_3 X_{11} X_4 \end{aligned}$$

$$\begin{aligned}
W_2 = & X_2X_9X_5 + X_1X_8X_4 + X_7X_{12}X_{14}X_{10} + X_3X_{11}X_{13}X_6 \\
& - X_2X_7X_{11}X_4 - X_1X_9X_{14}X_6 - X_8X_{13}X_{10} - X_3X_{12}X_5
\end{aligned}$$

After figuring out the rule for translating the edge labels one finds that the prepotentials in Eqs. (8.1) and (8.2) of [5] are $W_A = W_1$ and $W_B = W_2$.

For both superpotentials the surface \mathcal{M} has genus 1. Figures 18 and 19 in [5] show pictures of the planar periodic bi-partite graph which is the lifting of $\Gamma^{\bullet\circ}$ to the simply connected cover of \mathcal{M} .

One can not expect the Kasteleyn matrices K_A and K_B in [5] Eq. (8.3) to be the same as the bi-adjacency matrices \mathbb{K}_1^ϖ and \mathbb{K}_2^ϖ , respectively, because of the “untwist”. \mathbb{K}_1^ϖ and \mathbb{K}_2^ϖ are Kasteleyn matrices of the dimer models before the untwisting (see 8.2). Moreover Eqs. (8.4) and (8.5) of [5] show that the Newton polygons of the determinants of the Kasteleyn matrices K_A and K_B are different. On the contrary, for both \mathbb{K}_1^ϖ and \mathbb{K}_2^ϖ the determinant is a linear combination of the monomials

$$\mathbf{u}^{[3,3,1,0,0,1]}, \mathbf{u}^{[2,2,1,1,1,1]}, \mathbf{u}^{[1,1,1,2,2,1]}, \mathbf{u}^{[2,0,0,2,2,2]}, \mathbf{u}^{[3,1,0,1,1,2]}, \mathbf{u}^{[0,2,2,2,2,0]}, \mathbf{u}^{[1,3,2,1,1,0]}.$$

So, in agreement with Theorem 9.3, the Newton polygons of $\det \mathbb{K}_1^\varpi$ and $\det \mathbb{K}_2^\varpi$ coincide with the polygon in Figure 4 case B_8 and 3.7. In spite of having the same Newton polygon $\det \mathbb{K}_1^\varpi$ and $\det \mathbb{K}_2^\varpi$ are not equal; indeed when all weights are 1 they differ in the coefficient of $\mathbf{u}^{[2,2,1,1,1,1]}$.

10 Bi-adjacency matrix with critical weights and the principal \mathcal{A} -determinant

10.1. In [11] p.297 Eq. (1.1) Gelfand, Kapranov and Zelevinsky define for a set $\mathcal{A} = (\mathbf{a}_1, \dots, \mathbf{a}_N) \subset \mathbb{Z}^{k+1}$ as in 4.1 the *principal \mathcal{A} -determinant* $E_{\mathcal{A}}(f_{\mathcal{A}})$. The definition uses the Laurent polynomial

$$f_{\mathcal{A}} = \sum_{i=1}^N u_i \mathbf{x}^{\mathbf{a}_i}, \tag{33}$$

where $\mathbf{x}^{\mathbf{m}} = x_1^{m_1} x_2^{m_2} \dots x_{k+1}^{m_{k+1}}$ for $\mathbf{m} = (m_1, \dots, m_{k+1}) \in \mathbb{Z}^{k+1}$ and where the coefficients u_1, \dots, u_N are variables. The name “principal \mathcal{A} -determinant” refers to the fact ([11] p.298 Prop. 1.1) that $E_{\mathcal{A}}(f_{\mathcal{A}})$ can be written as the determinant of some exact complex, i.e.

$$E_{\mathcal{A}}(f_{\mathcal{A}}) = \prod_j (\det M_j)^{(-1)^j}$$

for certain matrices M_j . Another useful description of $E_{\mathcal{A}}(f_{\mathcal{A}})$ is given in [11] p.299 Prop. 1.2:

$$E_{\mathcal{A}}(f_{\mathcal{A}}) = \pm \prod_{\Gamma \subset \text{convex hull}(\mathcal{A})} \Delta_{\mathcal{A} \cap \Gamma}(f_{\mathcal{A} \cap \Gamma})^{m(\Gamma)} \quad (34)$$

where the product runs over all faces Γ of the primary polytope $\text{convex hull}(\mathcal{A})$ (cf. 4.12); $m(\Gamma)$ is a multiplicity and $\Delta_{\mathcal{A} \cap \Gamma}(f_{\mathcal{A} \cap \Gamma})$ is the $(\mathcal{A} \cap \Gamma)$ -discriminant of the Laurent polynomial $f_{\mathcal{A} \cap \Gamma} = \sum_{i: \mathbf{a}_i \in \Gamma} u_i \mathbf{x}^{\mathbf{a}_i}$. The latter discriminant is a polynomial in the variables u_i with $\mathbf{a}_i \in \Gamma$. To define it (see [11] p.271) one needs the algebraic set $\nabla_{\mathcal{A} \cap \Gamma}$ which is the closure in $\mathbb{C}^{\mathcal{A} \cap \Gamma}$ of:

$$\{\mathbf{u} \in \mathbb{C}^{\mathcal{A} \cap \Gamma} \mid \exists \mathbf{x}_0 \in (\mathbb{C}^*)^{k+1} \text{ s.t. } f_{\mathcal{A} \cap \Gamma}(\mathbf{x}_0) = \frac{\partial f_{\mathcal{A} \cap \Gamma}}{\partial x_i}(\mathbf{x}_0) = 0, \forall i\}.$$

Then, by definition, $\Delta_{\mathcal{A} \cap \Gamma}(f_{\mathcal{A} \cap \Gamma}) = 1$ if $\text{codim}_{\mathbb{C}^{\mathcal{A} \cap \Gamma}}(\nabla_{\mathcal{A} \cap \Gamma}) > 1$ and

$$\text{zero locus of } \Delta_{\mathcal{A} \cap \Gamma}(f_{\mathcal{A} \cap \Gamma}) = \nabla_{\mathcal{A} \cap \Gamma} \quad \text{if } \text{codim}_{\mathbb{C}^{\mathcal{A} \cap \Gamma}}(\nabla_{\mathcal{A} \cap \Gamma}) = 1.$$

So, $E_{\mathcal{A}}(f_{\mathcal{A}})$ gives the locus of the points $(u_1, \dots, u_N) \in \mathbb{C}^N$ for which at least one of the Laurent polynomials $f_{\mathcal{A} \cap \Gamma}$ has a critical point with critical value 0.

10.2. Theorem. ([11]p.302 Thm.1.4; cf.(17))

The Newton polytope of $E_{\mathcal{A}}(f_{\mathcal{A}})$ coincides with the secondary polytope $\Sigma(\mathcal{A})$. ■

10.3. Theorems 10.2 and 9.3 in combination with Formula (20) make one wonder whether for an appropriate choice of the weight ϖ the determinant of the bi-adjacency matrix \mathbb{K}^{ϖ} is equal to the principal \mathcal{A} -determinant $E_{\mathcal{A}}(f_{\mathcal{A}})$, up to the simple transformation necessitated by (20). In order to formulate this transformation we must make the dependence on u_1, \dots, u_N visible by writing $\mathbb{K}^{\varpi}(u_1, \dots, u_N)$ and $E_{\mathcal{A}}(f_{\mathcal{A}}(u_1, \dots, u_N))$.

After some experimenting with examples I found a very natural and simple choice for the weight that does the job.

10.4. Definition. The *critical weight* for the arrows of the quiver \mathbf{Q} is the function

$$\text{crit} : E \rightarrow \mathbb{Z}_{>0}, \quad \text{crit}(e) = \#\{e' \in E \mid s(e') = s(e), t(e') = t(e)\} \quad (35)$$

10.5. Conjecture. *For every set \mathcal{A} as in 4.1 and every dessin $(\mathcal{M}, \mathbf{Q})$ (see 6.18) constructed from \mathcal{A} by the algorithm in Section 6 the determinant of*

the bi-adjacency matrix with critical weight and the principal \mathcal{A} -determinant satisfy:

$$(u_1 \cdot \dots \cdot u_N)^{\text{vol}_{\mathcal{A}}} \det \mathbb{K}^{\text{crit}}(u_1^{-1}, \dots, u_N^{-1}) = E_{\mathcal{A}}(f_{\mathcal{A}}(u_1, \dots, u_N)). \quad (36)$$

10.6. Remark. In support of the above conjecture we can point out that the coefficients of the monomials corresponding to the vertices of the secondary polygons are, up to sign, the same for the two sides of Equation (36). Indeed, Theorem 1.4 of [11]p.302 gives the coefficient of the monomial in the principal \mathcal{A} -determinant which corresponds to a vertex of the secondary polytope. Such a vertex corresponds to a maximal cone C in the secondary fan. In the notations of Definition 3.3 the formula in loc. cit. for the coefficient of the monomial corresponding to C reads:

$$\pm \prod_{\{i,j\} \in L_C} |\det(\mathbf{b}_i, \mathbf{b}_j)|^{|\det(\mathbf{b}_i, \mathbf{b}_j)|}. \quad (37)$$

On the other hand, Theorems 7.2 and 9.3 show that the same vertex corresponds to a perfect matching P_C . From the role of perfect matchings in the computation of the determinant of the bi-adjacency matrix (see 9.1) one now easily checks that the coefficient of the monomial in the determinant, which corresponds to C , is (possibly up to sign) the same as (37).

In the remainder of this section we explicitly verify Conjecture 10.5 in some examples.

10.7. Example. For case $B_2 = \begin{bmatrix} 0 & 1 & 1 & -2 \\ -1 & 0 & 2 & -1 \end{bmatrix}$ in Figure 3 the algorithm in Section 6 yields in the following bi-adjacency matrix with critical weights:

$$\mathbb{K}^{\text{crit}} = \begin{bmatrix} 2u_1u_4 & 3u_3u_4 & u_1u_3 \\ 2u_2u_3 & u_2u_4 & 3u_3u_4 \\ u_1u_2 + 3u_3u_4 & 2u_2u_3 & 2u_1u_4 \end{bmatrix}.$$

One easily computes

$$\det \mathbb{K}^{\text{crit}} = 27\mathbf{u}^{[0,0,3,3]} + 4\mathbf{u}^{[1,2,3,0]} + 4\mathbf{u}^{[2,1,0,3]} - 18\mathbf{u}^{[1,1,2,2]} - \mathbf{u}^{[2,2,1,1]}$$

Note that the exponents are the same as the coordinates of the vertices and the interior point of the secondary polygon in 3.5. For the computation of the principal \mathcal{A} -determinant we note that in this case (see also Example 4.6)

$$\mathcal{A} = (\mathbf{a}_1, \mathbf{a}_2, \mathbf{a}_3, \mathbf{a}_4) = \left(\begin{bmatrix} 1 \\ 0 \end{bmatrix}, \begin{bmatrix} 1 \\ 3 \end{bmatrix}, \begin{bmatrix} 1 \\ 1 \end{bmatrix}, \begin{bmatrix} 1 \\ 2 \end{bmatrix} \right)$$

and hence $f_{\mathcal{A}} = x_1(u_1 + u_2x_2^3 + u_3x_2 + u_4x_2^2)$. The primary polytope is shown in Figure 2. The two boundary points of this primary polytope contribute factors u_1 and u_2 to the principal \mathcal{A} -determinant (cf. Equation (34)). The contribution from the full primary polytope is the very classical discriminant of the cubic polynomial $u_1 + u_3x_2 + u_4x_2^2 + u_2x_2^3$, which is (e.g. [11] p.405)

$$27u_1^2u_2^2 + 4u_1u_4^3 + 4u_3^3u_2 - u_3^2u_4^2 - 18u_1u_3u_4u_2.$$

Thus we find

$$E_{\mathcal{A}}(f_{\mathcal{A}}) = 27\mathbf{u}^{[3,3,0,0]} + 4\mathbf{u}^{[2,1,0,3]} + 4\mathbf{u}^{[1,2,3,0]} - \mathbf{u}^{[1,1,2,2]} - 18\mathbf{u}^{[2,2,1,1]}.$$

This shows that conjecture 10.5 holds in this case.

10.8. Example. When critical weights are used the two bi-adjacency matrices in Example 9.4 become

$$\mathbb{K}_1^{\text{crit}} = \begin{bmatrix} 2u_1u_2 & u_2u_4 & 0 & u_1u_4 \\ u_5u_6 & u_2u_6 & u_2u_5 & 0 \\ u_1u_6 + u_2u_3 & u_4u_6 & 2u_1u_2 & u_3u_4 \\ u_3u_5 & 0 & u_1u_5 & u_1u_3 \end{bmatrix}$$

$$\mathbb{K}_2^{\text{crit}} = \begin{bmatrix} 2u_1u_2 & u_2u_5 & 0 & u_1u_5 \\ u_1u_4 & 2u_1u_2 & u_2u_4 & 0 \\ u_2u_3 & u_5u_6 & u_2u_6 & u_3u_5 \\ u_3u_4 & u_1u_6 & u_4u_6 & u_1u_3 \end{bmatrix}$$

One easily computes $\det \mathbb{K}_1^{\text{crit}}$ and $\det \mathbb{K}_2^{\text{crit}}$ and finds that both are equal to

$$4\mathbf{u}^{[3,3,1,0,0,1]} + 2\mathbf{u}^{[1,1,1,2,2,1]} + \mathbf{u}^{[1,3,2,1,1,0]} + \mathbf{u}^{[3,1,0,1,1,2]} - \\ - \mathbf{u}^{[2,0,0,2,2,2]} - \mathbf{u}^{[0,2,2,2,2,0]} - 6\mathbf{u}^{[2,2,1,1,1,1]}.$$

This gives a remarkable contrast with the last line of Example 9.4 and underlines the role of the critical weight in making Conjecture 10.5 reasonable for every dessin obtained from \mathcal{A} .

Transforming the above determinant as in the left-hand side of Equation (36) yields

$$4\mathbf{u}^{[1,1,3,4,4,3]} + 2\mathbf{u}^{[3,3,3,2,2,3]} + \mathbf{u}^{[3,1,2,3,3,4]} + \mathbf{u}^{[1,3,4,3,3,2]} - \mathbf{u}^{[2,4,4,2,2,2]} - \\ - \mathbf{u}^{[4,2,2,2,2,4]} - 6\mathbf{u}^{[2,2,3,3,3,3]} \\ = u_1u_2u_3^2u_4^2u_5^2u_6^2(u_4u_5 - u_1u_2)(4u_3u_4u_5u_6 + u_2^2u_3^2 - 2u_1u_2u_3u_6 + u_1^2u_6^2). \quad (38)$$

From the matrix B_8 in Figure 4 one easily finds \mathcal{A} and the corresponding polynomial

$$f_{\mathcal{A}} = u_1x_1 + u_2x_1x_2 + u_3x_1x_3 + u_4x_1x_4 + u_5x_1x_2x_4^{-1} + u_6x_1x_2x_3.$$

The primary polytope $\text{convex hull}(\mathcal{A})$ is 3-dimensional and has seven 2-dimensional faces, six of which are triangles and one is a quadrangle. Its only integer points are its vertices and these correspond to the monomials of $f_{\mathcal{A}}$. One can compute the discriminants for the polynomials supported by the faces of the primary polytope and multiply these to get the principal \mathcal{A} -determinant $E_{\mathcal{A}}(f_{\mathcal{A}})$ as in Equation (34). The result is exactly as in (38), with the 4-term factor coming from the primary polytope itself, the 2-term factor coming from the quadrangle face and the other factors with multiplicities coming from the vertices. *This shows that conjecture 10.5 holds in this case.*

10.9. Further examples. Exactly as in Example 10.7 one can verify Conjecture 10.5 for other “four-nomials” of degree ≤ 5 (see Example 4.7) by using the formulas in [11] for discriminants of quartic and quintic polynomials.

The method of Example 10.8 can be successfully employed to verify Conjecture 10.5 for, for instance, cases B_5 , B_6 , B_{10} in Figure 4. It also works for $B = \begin{bmatrix} -3 & 1 & 1 & 1 & 0 & 0 & 0 \\ -3 & 0 & 0 & 0 & 1 & 1 & 1 \end{bmatrix}$ and $B = \begin{bmatrix} 1 & 1 & 0 & -2 & 0 \\ 0 & 0 & 1 & 1 & -2 \end{bmatrix}$, which are closely related to B_{16} and B_9 , respectively.

References

- [1] Benvenuti, S., S. Franco, A. Hanany, D. Martelli, J. Sparks, *An Infinite Family of Superconformal Quiver Gauge Theories with Sasaki-Einstein Duals*, JHEP 0506 (2005) 064; also arXiv:hep-th/0411264
- [2] Bruijn, N.G. de, *Algebraic theory of Penrose’s non-periodic tilings of the plane I*, Proceedings of the Koninklijke Nederlandse Akademie van Wetenschappen, Series A, vol 84 (= Indagationes Mathematicae, vol 43), 1981, 39-52
- [3] Feng, B., S. Franco, A. Hanany, Y-H. He, *Symmetries of Toric Duality* arXiv:hep-th/0205144
- [4] Feng, B., Y-H. He, K. Kennaway, C. Vafa, *Dimer Models from Mirror Symmetry and Quivering Amoebae*, arXiv:hep-th/0511287
- [5] Franco, S., A. Hanany, K. Kennaway, D. Vegh, B. Wecht, *Brane Dimers and Quiver Gauge Theories*, arXiv:hep-th/0511287
- [6] Franco, S., A. Hanany, D. Martelli, J. Sparks, D. Vegh, B. Wecht, *Gauge Theories from Toric geometry and Brane tilings*, arXiv:hep-th/0505211

- [7] Fulton, W., *Introduction to Toric Varieties*, Annals of Math. Studies, Study 131, Princeton University Press, 1993
- [8] Gelfand, I.M., A.V. Zelevinskii, M.M. Kapranov, *Hypergeometric functions and toral manifolds*, Functional Analysis and its Applications 23 (1989), 94-106
 [8]' correction to [8], Funct. Analysis and its Appl. 27 (1993) 295
- [9] Gelfand, I.M., M.M. Kapranov, A.V. Zelevinsky, *Generalized Euler Integrals and A- Hypergeometric Functions*, Advances in Math. 84 (1990), 255-271
- [10] Gelfand, I.M., A.V. Zelevinsky, M.M. Kapranov, *Equations of Hypergeometric Type and Newton Polyhedra*, Soviet Math. Dokl. 37 (1988), 678-683
- [11] Gelfand, I.M., M.M. Kapranov, A.V. Zelevinsky, *Discriminants, Resultants and Multidimensional Determinants*, Birkhäuser Boston, 1994
- [12] Hanany, A., C. Herzog, D. Vegh, *Brane Tilings and Exceptional Collections*, arXiv:hep-th/0602041
- [13] Hanany, A., K. Kennaway, *Dimer models and toric diagrams*, arXiv:hep-th/0503149
- [14] Hanany, A., D. Vegh, *Quivers, Tilings, Branes and Rhombi*, arXiv:hep-th/0511063
- [15] Kennaway, K., *Brane Tilings*, arXiv:0706.1660
- [16] Kenyon, R., *An introduction to the dimer model*, arXiv:math/0310326
- [17] Kenyon, R., A. Okounkov, S. Sheffield, *Dimers and Amoebae*, arXiv:math-ph/0311005
- [18] Lando, S., Zvonkin, A., *Graphs on Surfaces and Their Applications*, Encyclopedia of Math. Sciences vol. 141, subseries Low-Dimensional Topology vol. 11, Springer-Verlag, Berlin-Heidelberg, 2004.
- [19] Martelli, D., J. Sparks, *Toric Geometry, Sasaki-Einstein Manifolds and a New Infinite Class of AdS/CFT Duals*, Commun.Math.Phys. 262 (2006) 51-89; also arXiv:hep-th/0411238
- [20] Okounkov, A., N. Reshetikin, C. Vafa, *Quantum Calabi-Yau and Classical Crystals*, arXiv:hep-th/0309208

- [21] Poonen, B., F. Rodriguez-Villegas, *Lattice polygons and the number 12*, Am. Math. Monthly 107 (2000) p. 238-250
- [22] *The Grothendieck Theory of Dessins d'Enfants*, L. Schneps (ed.) London Math. Soc. Lecture Note Series 200, Cambridge University Press, 1994.
- [23] Senechal, M., *Quasicrystals and geometry*, Cambridge University Press, 1995.
- [24] Shabat, G., V. Voevodsky, *Drawing Curves Over Number Fields*, in: *The Grothendieck festschrift Volume III*, P. Cartier et. al. (eds), Progress in Mathematics vol. 88, Birkhäuser, Boston, 1990
- [25] Stienstra, J., *GKZ Hypergeometric Structures*, in: *Arithmetic and Geometry Around Hypergeometric Functions*, R-P. Holzapfel, A. M. Uludağ, M. Yoshida (eds.), Progress in Mathematics vol. 260, Birkhäuser, Basel, 2007, p. 313-371; see also math.AG/0511351
- [26] Sturmfels, B., *Gröbner Bases and Convex Polytopes*, University Lecture Series vol. 8, American Math. Soc., 1996